RESEARCH ARTICLE

High-performance eco-concrete beams with calcined montmorillonite, metakaolin pyrolyzed coffee grounds, and hybrid fibers for enhanced bending strength and microstructural refinement

Amani Abdallah Hepautwa[1,2]*, Askwar Hilonga[1], Register Mrosso[1], Tusekile Alfredy[1], Gabriel Mwalusambo[1,2], Fina Lesafi[1], Yusufu Abeid Chande Jande[1,3]

1 Department of Materials and Energy Sciences and Engineering, Nelson Mandela African Institution of Science and Technology, Arusha, Tanzania, **2** Department of Civil and Irrigation Engineering, Mwalimu Julius K. Nyerere University of Agriculture and Technology, Musoma (Butiama-HQ), Mara, Tanzania, **3** Water Infrastructure and Sustainable Energy Futures (WISE-Futures) African Centre of Excellence, The Nelson Mandela African Institution of Science and Technology, Arusha, Tanzania

* hepautwaamani@gmail.com

Citation: Hepautwa AA, Hilonga A, Mrosso R, Alfredy T, Mwalusambo G, Lesafi F, et al. (2026) High-performance eco-concrete beams with calcined montmorillonite, metakaolin pyrolyzed coffee grounds, and hybrid fibers for enhanced bending strength and microstructural refinement. PLoS One 21(3): e0334732. https://doi.org/10.1371/journal.pone.0334732

Editor: Parthiban Kathirvel, SASTRA Deemed University, INDIA

Received: October 1, 2025

Accepted: February 14, 2026

Published: March 5, 2026

Data availability statement: Data may be found in a manuscript.

Funding: MNUAT- HEET.

Abstract

This study investigates the flexural performance and microstructural evolution of reinforced concrete beams incorporating calcined montmorillonite (CMMT), metakaolin (MK), pyrolyzed coffee grounds (PCG), and hybrid fibers (steel or banana) as sustainable partial replacements for natural sand and cementitious binders. The replacement levels—12.5% SCM (CMMT or MK) and 15% PCG—were selected based on preliminary optimization trials and evidence from prior studies that identify these ranges as the threshold at which pozzolanic reactivity, workability, and particle packing achieve maximum benefit without compromising matrix integrity. Thirteen mix groups and a control beam were cast and tested under four-point bending, with three replicates per group. Statistical analysis using one-way ANOVA ($\alpha = 0.05$) confirmed significant differences in peak load, stiffness, ductility, and energy absorption across mixes ($p < 0.05$). Beams containing CMMT and 1.5% steel fibers achieved the highest flexural capacity, exhibiting a 92–105% increase in ultimate load relative to the control, while mixes with 1.0% banana fibers demonstrated the greatest ductility and post-cracking deformation capacity. Improvements in stiffness (up to 68%) and energy absorption (up to 120%) were closely linked to microstructural refinement observed through XRD and SEM. Quantitative indicators—including a 22–34% reduction in portlandite peak intensity, an increase in amorphous C–S–H content, and visibly compacted interfacial transition zones—corroborated the enhanced matrix densification induced by CMMT and PCG.The combined use of PCG, CMMT, and natural/steel fibers significantly reduced reliance on natural sand and cement while improving structural performance, demonstrating a viable pathway for developing high-performance eco-concretes for structural applications. Although direct durability

Competing interests: The authors have declared that no competing interests exist.

Abbreviations: CMMT, Calcined Montmorillonite; MK, Metakaolin; PCG, Pyrolyzed Coffee Grounds; SCM, Supplementary Cementitious Material; C-S-H, Calcium Silicate Hydrate; CH, Calcium Hydroxide; ITZ, Interfacial Transition Zone; SEM, Scanning Electron Microscopy; SSFM, Steel Fiber + SCM Modified Mix; BNFM, Banana Fiber + SCM Modified Mix; kN, Kilonewton; mm, Millimeter; kN/mm, Kilonewton per Millimeter.

tests were not conducted, the observed microstructural densification suggests potential improvements in long-term resistance to moisture and chloride ingress, warranting further research.

1. Introduction

Concrete production continues to face increasing environmental scrutiny due to the high carbon footprint associated with Portland cement and the depletion of natural river sand. In response, the incorporation of supplementary cementitious materials (SCMs) and recycled bio-based wastes has emerged as a promising strategy to reduce embodied CO_2 while enhancing the microstructural and mechanical performance of concrete. Calcined montmorillonite (CMMT) and metakaolin (MK) are among the most reactive aluminosilicate SCMs, offering high pozzolanic activity, improved packing density, and refined interfacial transition zones (ITZ). Recent studies have demonstrated their capacity to reduce portlandite content, densify the matrix, and improve mechanical performance in structural concretes [1–5]. Parallel to SCM development, the valorization of agricultural residues such as pyrolyzed coffee grounds (PCG) offers an additional sustainability benefit by replacing fine aggregates while improving internal curing and mitigating microcracking. PCG contains porous carbonaceous microstructures that enhance water retention, promote secondary hydration, and reduce environmental waste disposal challenges. Prior studies indicate that replacement levels around 10–20% optimize mechanical and microstructural performance while maintaining workable rheology, forming the basis for selecting 15% replacement in this study. Calcined Fiber reinforcement further extends the ductility, energy absorption, and post-cracking stability of concrete. Steel fibers significantly enhance load-carrying capacity and toughness, whereas natural fibers such as banana fibers improve crack bridging and deformation capacity at lower cost. Although these fibers are evaluated independently in literature, the term “hybrid fibers” within this study refers to the investigation of both steel-fiber-based mixes and banana-fiber-based mixes, rather than a blend of both fibers in the same mix. Despite extensive research on SCMS, PCG, and fibers individually, their combined use in reinforced concrete beams, especially with CMMT, remains largely unexplored [4–9]. Existing studies primarily focus on paste or mortar systems, or on plain concrete specimens, offering limited insight into structural-scale behavior under flexural loading. Moreover, few works integrate mechanical performance with quantitative microstructural analysis such as XRD peak intensity shifts, C–S–H development, CH depletion rates, or SEM-based ITZ densification metrics [5,6,9–16].

The interaction between PCG-induced internal curing, SCM-driven pozzolanic reactions, and fiber-matrix bond mechanisms also remains insufficiently documented. This gap hinders the design of high-performance eco-concrete beams for sustainable infrastructure [17–21].

To address these limitations, this study investigates the combined effects of CMMT or MK (12.5%), PCG (15%), and varying volumes of steel or banana fibers (0.5–1.5%) on the flexural behavior and microstructural characteristics of reinforced

concrete beams. The selected replacement levels are based on optimization evidence in prior literature and preliminary mix trials conducted to balance pozzolanic reactivity, workability, and density variation [1–4,7,22]. Structural-scale beams were tested under four-point loading, and mechanical responses—including peak load, stiffness, ductility, and energy absorption—were statistically evaluated using one-way ANOVA. Complementary XRD, EDX and SEM analyses were performed to quantify microstructural refinement and correlate phase transformation with mechanical response.

2. Materials and methods

2.1. Research framework and experimental workflow

The research followed a structured and integrated methodology designed to evaluate the mechanical and microstructural performance of reinforced concrete beams incorporating calcined montmorillonite (CMMT), pyrolyzed coffee grounds (PCG), and hybrid fibers. The workflow consisted of sequential and mutually reinforcing stages beginning with material characterization, followed by mix design, specimen preparation, mechanical testing, microstructural examination, and statistical validation. Each stage was aligned with the overall objective of establishing scientific, structural, and sustainability-driven justification for the performance of the modified concrete composites.

The study commenced with the physical and chemical characterization of cement, aggregates, CMMT, PCG, and the reinforcing fibers to establish the baseline material properties required for mix design. This was followed by the development of mix proportions using ACI 211.1 guidelines, with additional adjustments to account for the significantly different physical properties of PCG and the effect of CMMT on water demand and matrix density. Reinforced concrete beams were then cast according to the finalized mix proportions, incorporating varying fiber types and dosages to explore the influence of hybrid reinforcement systems.

All beams underwent a 28-day curing period prior to testing. Mechanical performance was assessed through four-point bending tests, where load–deflection responses were captured using high-resolution sensors. From these responses, flexural load capacity, stiffness, deflection characteristics, ductility index, energy absorption, and energy dissipation parameters were quantified according to established fracture mechanics procedures.

Microstructural evaluation of selected mixes was conducted using X-ray diffraction (XRD), scanning electron microscopy (SEM), and energy dispersive X-ray spectroscopy (EDX). These analyses provided insight into hydration product formation, ITZ refinement, porosity development, and fiber–matrix interaction mechanisms, enabling direct correlation between observed mechanical behavior and internal microstructural transformations.

One-way ANOVA and Tukey HSD post-hoc tests were performed on all mechanical parameters to determine statistical significance among the mixes. The inclusion of F-values, p-values, and degrees of freedom strengthened the reliability of the comparisons and for more transparent statistical reporting.

The entire research pathway—from raw material preparation to microstructural and statistical validation—is illustrated in Fig 1, which provides a clear overview of the logical progression used to achieve the objectives of this study.

2.1.1. Cement and binders. Ordinary Portland Cement (OPC, 42.5R grade) was used as the primary binder for all mixtures. The selection of this cement type ensured consistent hydration behavior and compatibility with supplementary cementitious materials (SCMs). The physical and chemical characteristics of the cement were established through X-ray fluorescence (XRF) and Blaine fineness testing to provide a baseline for understanding how the introduction of calcined montmorillonite (CMMT) and pyrolyzed coffee grounds (PCG) altered the hydration processes and microstructural development.

Calcined montmorillonite (CMMT) was produced by thermally activating raw montmorillonite clay at 750 °C, a temperature known to induce dehydroxylation and structural collapse, thereby enhancing its pozzolanic reactivity. The activated CMMT was expected to react with calcium hydroxide released during cement hydration, forming additional secondary C–S–H and contributing to matrix densification. Its inclusion at 12.5% by weight of cement was based on prior studies demonstrating optimal pozzolanic efficiency and improved mechanical performance at this replacement level. XRF analysis confirmed significant contents of SiO_2 and Al_2O_3, supporting its function as a reactive aluminosilicate source.

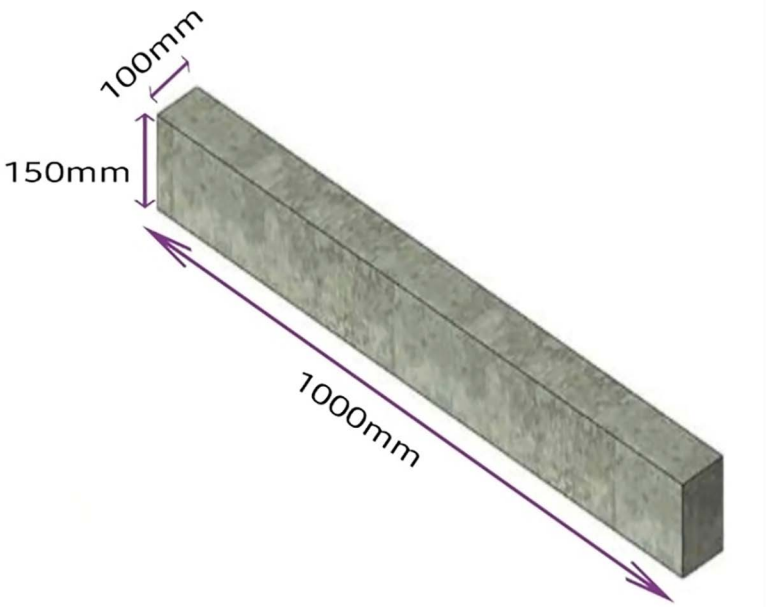

Fig 1. Dimensions of the concrete beam specimen.

https://doi.org/10.1371/journal.pone.0334732.g001

The pyrolyzed coffee grounds (PCG) used in this study resulted from controlled pyrolysis at 350 °C, which produced a fine biochar-like powder with enhanced internal porosity, reduced volatile content, and improved filler characteristics. When used as a 15% replacement of fine aggregates, the PCG was expected to improve particle packing, reduce porosity, and contribute to micro-filling within the cementitious matrix. BET surface area measurements and particle size distribution confirmed that the PCG possessed a porous microstructure capable of improving moisture retention during hydration and enhancing interfacial bonding with the C–S–H gel.

The combined use of OPC, CMMT, and PCG was designed to exploit both pozzolanic and micro-filling mechanisms, with the expectation of generating a refined matrix structure, reduced CH content, and enhanced interfacial transition zone (ITZ) performance. These binder characteristics formed the foundation for the mechanical and microstructural improvements evaluated in subsequent sections.

Table 1 presents the chemical composition of OPC, CMMT, and PCG as determined by XRF, providing a quantitative reference for understanding the contributions of each binder component to the observed performance enhancements.

2.1.2. Aggregates. Crushed granite was used as the coarse aggregate, while natural river sand served as the fine aggregate for all concrete mixtures. Both aggregates were evaluated in accordance with ASTM C127 and ASTM C128 to determine their specific gravity, water absorption, and particle size distribution, ensuring conformity with structural concrete requirements. Sieve analysis was performed following ASTM C136 to classify grading characteristics and verify compliance with standard concrete workability and packing density criteria.

The coarse aggregate was well-graded, angular, and free from deleterious materials, contributing to improved interlocking and enhanced load transfer within the composite. The fine aggregate exhibited a fineness modulus within the acceptable range (2.6–2.8), providing uniform particle packing and stability across mixtures. These baseline properties were essential for accurately assessing the effects of pyrolyzed coffee grounds (PCG) replacement on fine aggregate behavior.

To accommodate the introduction of PCG at 15% replacement of fine aggregates, corrections were made to account for the lower density and higher water absorption characteristics of PCG compared to natural sand. This

Table 1. Chemical composition of OPC, CMMT, and PCG (XRF Analysis).

Oxide Component (%)	OPC	CMMT (Calcined at 750°C)	PCG (Pyrolyzed at 350°C)
SiO_2	20.5	52.3	14.8
Al_2O_3	5.3	18.6	3.2
Fe_2O_3	3.8	6.5	1.1
CaO	63.4	4.7	2.5
MgO	2.1	3.9	1.4
K_2O	0.7	2.4	1.2
Na_2O	0.2	0.8	0.4
LOI	3.5	7.1	64.0
Other minor oxides	0.5	3.7	1.4

https://doi.org/10.1371/journal.pone.0334732.t001

adjustment ensured consistent fresh-state performance and prevented unintended variations in the water–cement ratio.

All aggregates were oven-dried to a constant mass at 105 °C before mixing to eliminate moisture variability. Their physical properties, including specific gravity, bulk density, and water absorption, were quantified and used for mix proportion calibration. These parameters are summarized in Table 2, providing a clear reference for the aggregate contributions to concrete performance and enhancing the reproducibility of the study.

2.1.3. Pyrolyzed coffee grounds (PCG), metakaolin (MK), and calcined montmorillonite (CMMT). The physical properties of the three materials used in this study reflect their distinct roles and combined influence on the behavior of the concrete composite. Pyrolyzed coffee grounds (PCG) exhibit a low specific gravity, high water absorption, and a porous internal structure, characteristics that classify them as a lightweight, highly absorbent fine material. These features allow PCG to function as an internal curing agent and micro-filler. Its high porosity enables the absorption of mixing water that is subsequently released during hydration, promoting improved moisture availability within the matrix. This contributes to reduced shrinkage, enhanced hydration, and better microstructural development. The wide particle size distribution of PCG also helps improve packing density when combined with natural sand.

Metakaolin (MK), in contrast, is a highly refined, fine powder with a significantly higher specific gravity and lower water absorption than PCG. Its high surface area and fine particle size enhance its reactivity, enabling it to participate actively in pozzolanic reactions with calcium hydroxide released during cement hydration. This contributes to the formation of secondary calcium silicate hydrate phases, which improve matrix density, reduce porosity, and strengthen the interfacial transition zone. The physical properties of MK demonstrate that it behaves predominantly as a chemically reactive supplemental cementitious material rather than as a lightweight filler as shown in Table 3.

Table 2. Physical properties of coarse and fine aggregates.

Property	Coarse Aggregate (Granite)	Fine Aggregate (River Sand)
Specific gravity (SSD)	2.68	2.62
Bulk density (kg/m³)	1550	1620
Water absorption (%)	0.7	1.2
Fineness modulus	—	2.65
Maximum size (mm)	20	4.75
Moisture content (%)	0.3	0.5
Shape characteristics	Angular	Rounded to sub-angular
Compacted void ratio (%)	40.5	36.0

https://doi.org/10.1371/journal.pone.0334732.t002

Table 3. Physical properties of PCG, metakaolin (MK), and calcined montmorillonite (CMMT).

Property	PCG (Pyrolyzed at 350°C)	Metakaolin (MK)	Calcined Montmorillonite (CMMT)
Specific gravity	1.25	2.60	2.58
Bulk density (kg/m³)	520	420	450
BET surface area (m²/g)	18.2	14–20	35–60
Particle size range (μm)	75–600	< 45	< 75
Water absorption (%)	8.4	1.2	2.8
pH (water suspension)	6.7	5–6	8–9
Bulk appearance	Dark, porous, irregular	Fine, off-white powder	Fine, light pink to tan powder
Surface texture	Rough, porous	Smooth, fine	Plate-like, micro-layered
Typical role in concrete	Filler, internal curing	Pozzolanic binder	Nucleation and densification
Density classification	Lightweight	Normal weight	Normal weight

https://doi.org/10.1371/journal.pone.0334732.t003

Calcined montmorillonite (CMMT) shares several similarities with MK in terms of fineness and density but differs significantly in surface texture and internal structure. The plate-like morphology of CMMT and its micro-layered surface contribute to improved packing and enhanced nucleation sites for hydration products. While its water absorption remains moderate, its physical structure supports pore refinement and contributes to improved microstructural continuity. These characteristics enable CMMT to complement MK by promoting densification through both physical and chemical mechanisms.

Together, the physical properties of these materials explain the synergistic behavior observed in the modified concrete mixtures. PCG contributes lightweight internal curing and micro-filling; MK provides high reactivity and matrix strengthening; and CMMT enhances packing, nucleation, and microstructural refinement. The integration of these materials results in improved flexural performance, enhanced energy absorption, and superior crack resistance, aligning with the mechanical and microstructural results reported in the study.

2.1.4. Fiber reinforcements. Two types of fibers—steel fibers and banana fibers—were incorporated into the concrete mixtures to evaluate the influence of hybrid reinforcement systems on flexural performance, ductility, and fracture energy. Both fiber types were selected to represent contrasting mechanical behaviors: high-modulus metallic reinforcement and low-modulus natural reinforcement, enabling a broader evaluation of composite behavior under bending loads.

The steel fibers used in this study were hooked-end, commercially manufactured high-strength microfibers with a length of 35 mm, diameter of 0.55 mm, aspect ratio of approximately 65, and tensile strength exceeding 1100 MPa. Their high stiffness and superior crack-bridging capacity provide substantial resistance to crack initiation and propagation, enhancing both strength and toughness. Their inclusion at 0.5%, 1.0%, and 1.5% volume fractions allowed for the assessment of dosage-dependent improvements in flexural stiffness, peak load, and post-cracking stability.

Banana fibers were sourced locally from processed banana pseudo-stems, manually extracted, cleaned, sun-dried, and cut to a uniform length of 30–35 mm. These natural lignocellulosic fibers possess moderate tensile strength and high elongation capacity, enabling significant post-cracking deformation and energy dissipation through gradual fiber pull-out mechanisms. Their density is markedly lower than steel fibers, resulting in improved crack distribution but reduced stiffness contribution. Banana fibers were also incorporated at 0.5%, 1.0%, and 1.5% volume fractions to systematically evaluate their influence on ductility and fracture energy.

All fibers were manually dispersed during the mixing process to ensure uniform distribution and minimize clustering. The contrasting properties of steel and banana fibers enabled a comprehensive evaluation of stiffness-driven versus ductility-driven reinforcement mechanisms within the PCG–CMMT-modified concrete matrix.

The mechanical and physical characteristics of the fibers—including tensile strength, modulus of elasticity, diameter, length, density, and water absorption behavior—are summarized in Table 4, facilitating reproducibility and reflecting the quantifiable differences that influenced the flexural behavior of the beams.

Table 4. Mechanical and physical properties of steel fibers and banana fibers.

Property	Steel Fibers	Banana Fibers
Length (mm)	35	30–35
Diameter (mm)	0.55	0.20–0.30
Aspect ratio	65	120–150
Tensile strength (MPa)	1100–1300	250–350
Elastic modulus (GPa)	200	8–12
Density (kg/m³)	7850	1350
Water absorption (%)	0	10–12
Surface texture	Hooked-end, smooth	Rough, lignocellulosic
Thermal stability	High	Moderate
Typical failure mode	Rupture or pull-out	Pull-out or fibrillation

https://doi.org/10.1371/journal.pone.0334732.t004

2.2. Mix design and proportioning

The concrete mix proportions were developed using the ACI 211.1 methodology for normal-weight concrete and subsequently modified to incorporate calcined montmorillonite (CMMT), pyrolyzed coffee grounds (PCG), and varying fiber dosages. The target compressive strength for mix design was 30–35 MPa, ensuring structural relevance for flexural beam applications. Initial trial batches were conducted to calibrate water content, adjust for PCG's high water absorption, and verify the workability range suitable for reinforced beam casting.

CMMT was incorporated at a fixed replacement level of 12.5% by mass of cement. This proportion was selected based on previous research indicating optimal pozzolanic reactivity, matrix densification, and mechanical performance at substitution between 10–15%. At 12.5%, the mix achieved a balance between improved microstructural refinement and minimal adverse effects on fresh-state properties. Pyrolyzed coffee grounds were used to replace 15% of fine aggregates by mass. This value was selected because preliminary trials and past studies demonstrated that PCG contents above 20% significantly reduce workability and cause excessive entrapped air, whereas contents below 15% underutilize the micro-filling benefits of PCG's porous internal structure.

Adjustments to the mix proportions were necessary due to the significantly lower specific gravity and higher absorption characteristics of PCG relative to natural sand. Water correction factors were applied to maintain a consistent effective water–cement ratio across mixtures. Similarly, incorporation of CMMT increased water demand due to its high surface area; therefore, a controlled superplasticizer dosage was introduced to maintain the slump within the workable range (60–80 mm).

The fiber-reinforced mixes were categorized into two primary groups: steel fiber mixes (SSFM1, SSFM2, SSFM3) and banana fiber mixes (BNFM1, BNFM2, BNFM3), corresponding to fiber volume fractions of 0.5%, 1.0%, and 1.5%, respectively. A control mixture containing no SCMs, PCG, or fibers was also included to provide baseline comparison. All mix constituents were batched by weight, and the mixing procedure followed ASTM C192, incorporating a staged addition of fibers to prevent clustering and promote uniform dispersion.

The final mix proportions for all mixtures—including cement, CMMT, fine and coarse aggregates, PCG, water, and fiber content—are summarized in Table 5, providing a transparent overview of material quantities and facilitating reproducibility of the experimental program.

2.3. Beam fabrication and reinforcement design

Reinforced concrete beams were prepared to evaluate the flexural performance of mixes modified with CMMT, pyrolyzed coffee grounds (PCG), and fiber reinforcement. All beams measured 150 mm × 200 mm × 1200 mm, with an effective span of 1000 mm during testing. The beam dimensions were selected to promote flexural-dominated behavior under four-point loading while ensuring compatibility with laboratory testing equipment and ASTM standards.

Table 5. Concrete mix proportions for all mixtures (kg/m³).

Component (kg/m³)	Control	SSFM1	SSFM2	SSFM3	BNFM1	BNFM2	BNFM3
Cement	380	380	380	380	380	380	380
CMMT (12.5%)	48	48	48	48	48	48	48
Water	190	190	190	190	190	190	190
Fine aggregate	650	553	553	553	553	553	553
PCG (15%)	115	115	115	115	115	115	115
Coarse aggregate	1100	1100	1100	1100	1100	1100	1100
Superplasticizer	4.0	4.0	4.0	4.0	4.0	4.0	4.0
Fiber content (%)	0	0.5	1.0	1.5	0.5	1.0	1.5
Steel fibers	0	39	78	117	0	0	0
Banana fibers	0	0	0	0	8	16	24

https://doi.org/10.1371/journal.pone.0334732.t005

Reinforcement layout and failure-mode control. Each beam was reinforced with two tensile steel bars (Ø12 mm) placed at the bottom and two compression bars (Ø10 mm) at the top, complemented by 8 mm diameter closed stirrups spaced at 100 mm centers along the entire length. The arrangement was designed to intentionally promote flexural failure rather than shear failure.

Flexural capacity was verified using standard reinforced concrete design principles, ensuring that the tensile reinforcement ratio remained within the under-reinforced domain to guarantee ductile flexural behavior. Shear capacity checks were performed by ensuring that the provided stirrups exceeded the minimum required shear reinforcement according to ACI 318. This eliminated the possibility of premature shear failure and ensured that the observed behavior during testing corresponded directly to the influence of material modifications rather than structural detailing.

Mixing, casting, and compaction. All concrete batches were mixed following ASTM C192, as illustrated in Fig 1, which presents the standardized sequence used throughout the study. Dry materials were first blended for 2 minutes to achieve uniform distribution of cementitious components and aggregates. As shown in Fig 1, water and chemical admixtures were then introduced gradually to control the rheology of the mixture and prevent lump formation. Fibers were incorporated slowly during the mixing stage to ensure uniform dispersion and minimize the clustering effects that were observed during initial trials. This gradual incorporation process, highlighted in Fig 1, facilitated a homogeneous and workable composite matrix.

Once the mixture reached a homogeneous consistency, it was cast into steel molds in two equal layers, as demonstrated in Fig 2. Layered casting was adopted to promote uniform density and reduce internal voids, ensuring consistency across all cube, cylinder, and beam specimens. Each layer was placed carefully to avoid disturbing the previous one, allowing proper compaction and geometric uniformity.

Compaction was performed using a table vibrator, as illustrated in Fig 3. Controlled vibration helped eliminate entrapped air, reduced honeycombing, and enhanced particle packing within the matrix. The vibration process shown in Fig 3 ensured full consolidation without causing segregation or bleeding. This step significantly improved the specimen integrity and supported reliable mechanical, durability, and microstructural evaluation.

Surface finishing and demolding. After casting, the surface of each beam was leveled and finished to a smooth texture to ensure consistent contact during bending tests. All beams were demolded after 24 hours under controlled laboratory conditions (~25 °C), after which they were transferred to the curing tank. This step significantly improved the specimen integrity and supported reliable mechanical, durability, and microstructural evaluation

2.4. Curing conditions

All concrete beams were subjected to a standardized curing regime immediately after demolding to ensure consistent hydration and to minimize variability in mechanical performance. After casting, the specimens remained in their molds for

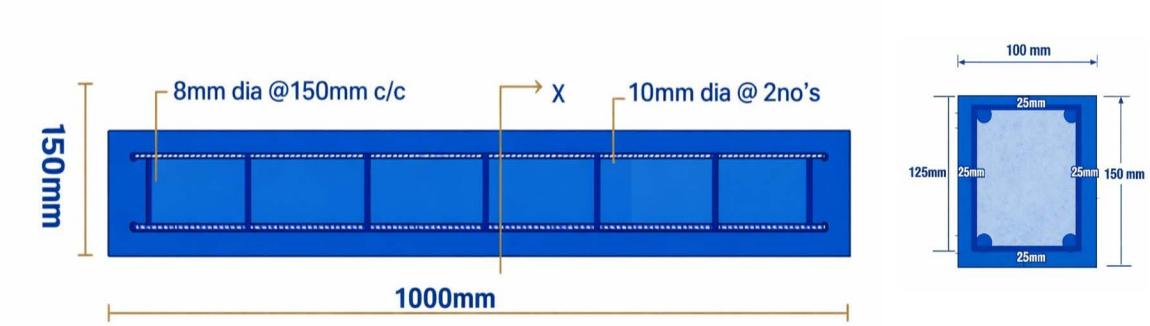

Fig 2. Reinforcement detailing of the concrete beam specimen.

https://doi.org/10.1371/journal.pone.0334732.g002

24 hours under laboratory conditions maintained at 23–25 °C and approximately 60% relative humidity. This initial curing period allowed for adequate early-stage strength development prior to handling.

After demolding, all beams were fully submerged in a temperature-controlled water-curing tank maintained at 23 ± 2 °C, in accordance with ASTM C511 recommendations for moist curing of cementitious materials. The curing duration was 28 days for all mixtures, ensuring that the hydration process reached a mature and stable phase prior to mechanical and microstructural testing. Water within the curing tank was replenished weekly to maintain consistency in mineral content, alkalinity, and temperature, preventing the formation of stagnant or contaminated conditions that could influence hydration kinetics.

The use of a controlled water-curing regime was particularly important given the presence of supplementary cementitious materials (CMMT) and the porous nature of the pyrolyzed coffee grounds (PCG). These constituents exhibit higher water demand and internal curing potential, making consistent curing conditions essential for isolating the true material effects on mechanical performance. Maintaining uniform curing between the control and modified mixes ensured that any observed differences in strength, stiffness, ductility, or energy parameters could be attributed to the material modifications rather than inconsistencies in hydration.

This controlled curing methodology ensures that the mechanical results accurately reflect the performance characteristics of the developed eco-concrete beam mixtures.

2.5. Mechanical testing procedures

Mechanical testing of the reinforced concrete beams was conducted to evaluate the influence of calcined montmorillonite (CMMT), pyrolyzed coffee grounds (PCG), and hybrid fibers on flexural behavior. All beams were tested after 28 days of curing to ensure stable hydration and eliminate early-age variability. The procedures followed in this study were developed to provide accurate and reproducible measurement of load–deflection behavior, crack propagation, and energy-based parameters that reflect both pre-peak and post-peak structural performance.

2.5.1. Workability assessment. The slump test was performed in accordance with ASTM C143 to assess fresh concrete consistency before casting. Maintaining consistent slump was essential to ensure identical placing and compaction across all mixtures, particularly because the introduction of PCG and CMMT alters water demand and internal friction within the mix. For all mixtures, superplasticizer dosage was adjusted during trial batches to achieve a target slump of 60–80 mm, ensuring proper fiber dispersion and minimizing segregation. Slump testing also ensured the comparability of results across fiber-reinforced and non-fiber mixes.

2.5.2. Four-point bending test setup. Flexural testing was conducted using a servo-controlled universal testing machine equipped with a 500 kN load cell. The beams were positioned on simple supports with an effective span of

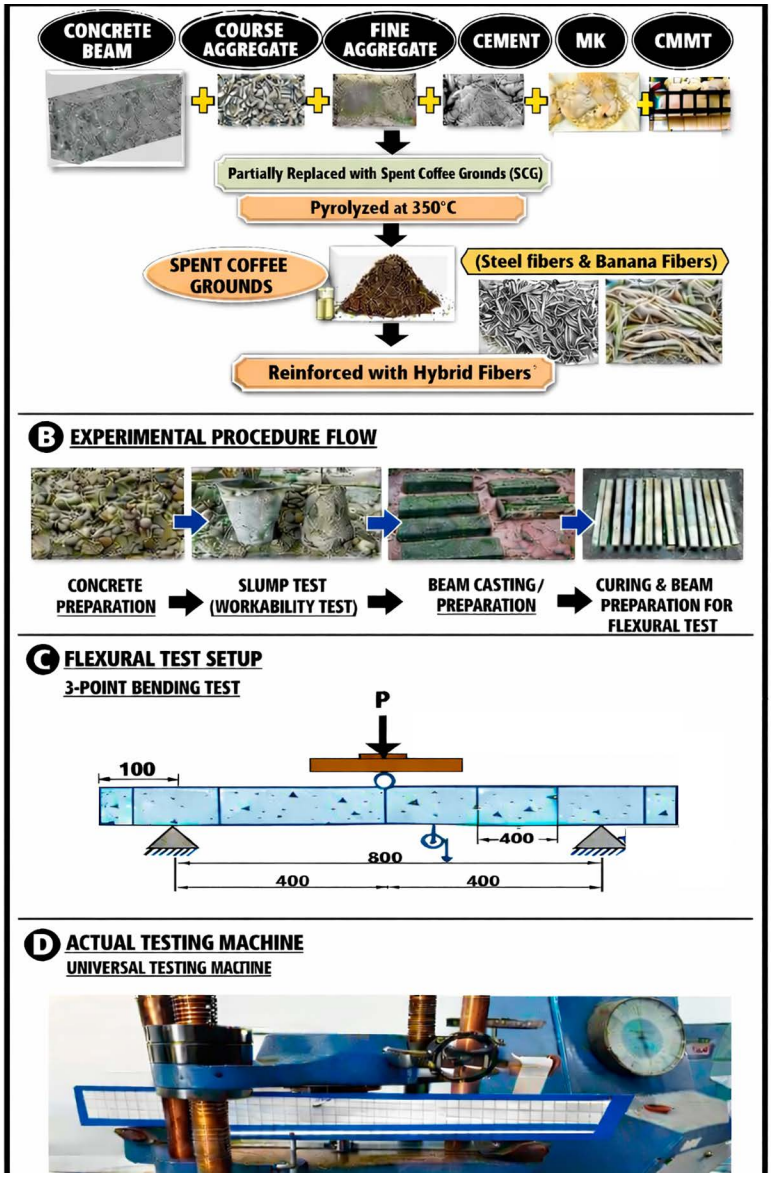

Fig 3. Schematic overview of materials and experimental procedure for eco-concrete beam preparation and flexural testing.

https://doi.org/10.1371/journal.pone.0334732.g003

1000 mm, as required to induce a pure bending region between the loading points. The four-point loading configuration, performed in accordance with ASTM C1609 and ASTM C78, ensured that shear influence was minimized and that the primary response measured was due to bending stresses.

The load was applied in displacement control mode at a constant loading rate of 0.5 mm/min, which allowed precise capture of both elastic and post-elastic behavior, including softening and residual strength. This rate was selected to avoid dynamic effects and to ensure a stable cracking response.

To capture mid-span deflection with high accuracy, a Linear Variable Differential Transformer (LVDT) with ±0.001 mm resolution was installed at the midpoint of the beam. Additional LVDTs were placed near the supports for select specimens to validate rotation and boundary conditions, ensuring that deflection measurements were free from undesired support

settlement. Data acquisition was performed using a digital logging system recording at 10 Hz to produce smooth, continuous load–deflection curves.

2.5.3. Pre-test conditioning and alignment. Before each test, beams were allowed to stabilize at laboratory temperature for at least two hours to minimize thermal gradients. The testing frame alignment was checked to ensure uniform load distribution across the loading heads. Minor surface irregularities on supports were corrected using a thin neoprene pad to eliminate stress concentrations.

Load heads and supports were lubricated lightly to maintain boundary conditions consistent with simply supported beams. Each beam was centrally aligned beneath the loading points using a laser-guided alignment tool to ensure accurate placement, minimizing eccentricity effects that could affect bending behavior.

2.5.4. Data recording and flexural response monitoring. Throughout the test, load and deflection data were continuously recorded. The initial linear segment of the load–deflection curve was used to determine flexural stiffness, while the peak load represented the flexural capacity. Deflection at peak load was used to compute ductility index, and the entire area under the curve—up to and beyond peak—was used to quantify energy absorption and post-peak energy dissipation.

Crack initiation, propagation, and failure patterns were visually documented using a high-resolution digital camera. This provided internal verification of structural performance and supported the microstructural discussion in the results section.

All beams were observed to fail in flexure through controlled crack formation in the pure bending region, confirming the appropriateness of the reinforcement design and validating that no specimen experienced premature shear failure.

2.5.5. Figure reference. The complete experimental setup, including support spacing, loading configuration, LVDT placement, and instrumentation layout, is illustrated in Fig 3. This figure ensures methodological transparency.

2.6. Calculation of flexural parameters

The flexural performance of the beams was evaluated from the load–deflection curves obtained during four-point bending. All formulas were applied consistently across mixtures to ensure accuracy and reproducibility.

2.6.1. Flexural load capacity. Flexural load capacity was defined as the maximum load recorded by the load cell during testing.

Formula:

$$\text{Pmax} = \text{maximum recorded load } (\text{kN})$$

This value represents the highest bending resistance prior to major cracking.

2.6.2. Flexural stiffness. Initial flexural stiffness was calculated from the slope of the linear portion of the load–deflection curve, taken between approximately 10 percent and 40 percent of the peak load.

Formula:

$$\text{K} = \frac{(\text{P2} - \text{P1})}{(\delta 2 - \delta 1)}$$

where P1 and P2 are load values within the linear region, and δ1 and δ2 are the corresponding mid-span deflections. Stiffness is expressed in kN per mm.

2.6.3. Mid-span deflection. Mid-span deflection at peak load was determined directly from the LVDT data.

Formula:

$$\delta_{max} = \text{deflection at } P_{max} \ (\text{mm})$$

This value reflects the deformation capacity at maximum bending resistance.

2.6.4. Ductility index. The ductility index measures the deformation capacity beyond the elastic range.

The yield point was taken as the end of the linear region of the load–deflection curve.

The failure point corresponds to the deflection at which the load decreased to about 10 percent of P_{max}.

Formula:

$$DI = \frac{\delta failure}{\delta yield}$$

2.6.5. Energy absorption. Energy absorption represents the total mechanical work done on the beam from the start of loading to the peak load.

It was computed as the area under the ascending portion of the load–deflection curve using the trapezoidal rule.

Formula:

$$Ea = \Sigma \frac{(Pi + Pi+1)}{2} \times (\delta i + 1 - \delta i)$$

Energy absorption is expressed in kN·mm.

2.6.6. Energy dissipation. Energy dissipation represents the post-peak toughness and was calculated as the area under the descending portion of the load–deflection curve until failure.

Formula:

$$Ed = \Sigma \frac{(Pi + Pi+1)}{2} \times (\delta i + 1 - \delta i)$$

The summation begins at the peak load point and ends at the point where the load dropped to approximately 10 percent of P_{max}.

2.6.7. Failure definition and curve segmentation. The failure point ($\delta_{failure}$) was defined as the deflection at which the load decreased to about 10 percent of the peak load. This definition was used consistently across all specimens.

The load–deflection curve was segmented as follows:

- Ascending branch (elastic region and microcrack formation)
- Peak load point (P_{max})
- Descending branch (macro-cracking and fiber pull-out mechanisms)

These definitions allow consistent calculation of stiffness, ductility, energy absorption, and energy dissipation.

2.7. Microstructural characterization methods

Microstructural analysis was conducted to understand the internal mechanisms responsible for the mechanical behavior of the PCG–CMMT–fiber-reinforced concretes. Selected specimens from the control, steel-fiber mixes, and banana-fiber mixes were examined to evaluate matrix refinement, fiber–matrix bonding, porosity changes, and hydration product development. Three techniques were used: X-ray diffraction (XRD), scanning electron microscopy (SEM), and energy-dispersive X-ray spectroscopy (EDX).

2.7.1. X-ray diffraction (XRD). XRD analysis was performed to identify crystalline hydration products and quantify changes associated with the incorporation of calcined montmorillonite and pyrolyzed coffee grounds. Powdered samples were collected from crushed beam fragments taken from the constant-moment region. Each sample was oven-dried at 60°C to remove moisture before testing.

The XRD scans were carried out using a diffractometer operating with Cu-Kα radiation at 40 kV and 30 mA. The scanning range was 5° to 60° 2θ, with a step size of 0.02° and a scan speed of 2° per minute. These settings allowed accurate identification of characteristic peaks such as calcium hydroxide, calcium silicate hydrate, quartz, and unreacted binder phases.

Relative peak intensities were used to compare the reduction of portlandite and the development of amorphous phases between mixes. These values supported the interpretation of improved pozzolanic activity, matrix densification, and microstructural refinement, which were later correlated with mechanical test results.

2.7.2. Scanning electron microscopy (SEM). SEM was used to examine fracture surfaces, evaluate fiber–matrix interaction, and observe microstructural features such as pore distribution, microcracks, and interfacial transition zone (ITZ) morphology.

Samples were cut from the tension zone of broken beams, dried, and coated with gold to ensure electrical conductivity. Imaging was performed under high vacuum at magnifications ranging from 200x to 5000x.

SEM observations allowed the identification of beneficial features such as improved ITZ compactness in CMMT-modified mixes, micro-filling effects of PCG particles, and evidence of fiber bridging and pull-out mechanisms. These microstructural findings provided direct support for mechanical performance improvements such as increased ductility and enhanced energy dissipation.

2.7.3. Energy-dispersive X-ray spectroscopy (EDX). EDX analysis was conducted alongside SEM imaging to determine the elemental composition of selected regions. The analysis enabled detection of calcium, silicon, aluminum, and carbon, which were used to interpret hydration behavior and pozzolanic activity.

Elemental maps were used to compare the Ca/Si ratio between the control and modified concrete mixes. Lower Ca/Si ratios indicated enhanced formation of secondary C–S–H in mixes containing CMMT and PCG. Carbon distributions were also evaluated to verify the presence and dispersion of PCG particles within the matrix.

2.7.4. Sample selection and comparative approach. Microstructural testing was performed on the control mix, the highest-performing steel fiber mix, and the highest-performing banana fiber mix to illustrate the differences produced by each modification strategy. This comparative selection ensured direct linkage between microstructural features and the statistically significant mechanical results presented.

2.8. Statistical analysis

Statistical analysis was carried out to determine whether the differences observed among the concrete mixtures were statistically significant. All mechanical parameters obtained from flexural testing, including flexural load capacity, stiffness, mid-span deflection, ductility index, energy absorption, and energy dissipation, were analyzed statistically to ensure reliability and scientific rigor.

The analysis was performed using one-way analysis of variance (ANOVA), followed by Tukey's Honestly Significant Difference (HSD) post-hoc test to identify specific pairwise differences between mixtures. A significance level of 0.05 was used for all evaluations.

2.8.1. One-way ANOVA procedure. One-way ANOVA was applied separately to each mechanical parameter to determine whether the mean values of different mixtures originated from the same population or if statistically significant differences existed.

The general ANOVA model used was:

$$F = \frac{\text{MSbetween}}{\text{MSwithin}}$$

where $MS_{between}$ is the mean square between groups and MS_{within} is the mean square within groups.

Degrees of freedom were calculated as follows:

$$df_{between} = k - 1$$

$$df_{within} = N - k$$

where k is the number of mix categories and N is the total number of specimens tested.

The p-value associated with each F-statistic was used to determine whether the observed differences were statistically meaningful. A p-value less than 0.05 indicated significant variation among mixtures.

2.8.2. Post-Hoc comparison (Tukey HSD). When ANOVA indicated significant differences, Tukey HSD was applied to compare all mixture pairs.

The Tukey HSD value was calculated as:

$$HSD = \frac{\sqrt{MSwithin}}{n}$$

where q is the studentized range statistic and n is the number of specimens per group.

If the absolute difference between two group means exceeded the HSD value, the difference between those mixtures was considered statistically significant.

This method identified which mixtures contributed to overall ANOVA significance and allowed grouping of mixes based on similarity or superiority in flexural performance.

2.8.3. Reporting format. The statistical results for each mechanical parameter were reported in a standardized format to ensure clarity, transparency for every parameter analyzed, the outputs included the F-value, the corresponding p-value, the degrees of freedom for both the between-group and within-group variations, the Tukey grouping letters identifying statistically similar or different mixtures, and the specific pairs of mixtures that showed significant differences. Presenting the results in this structured manner It also ensures that all conclusions drawn from the mechanical performance data are supported by rigorous and traceable statistical analysis.

2.8.4. Software and data handling. All statistical calculations were performed using standard statistical software capable of generating ANOVA tables and Tukey pairwise comparisons. Raw load–deflection data were exported directly from the digital acquisition system to ensure that no filtering or smoothing altered the statistical validity of the results.

2.8.5. Purpose and relevance. The use of ANOVA and post-hoc testing ensured that all differences reported in the results and discussion sections were supported by statistical evidence rather than descriptive interpretation. This approach allowed transparent comparison between the control mix and all modified mixes and ensured scientific accountability for claims related to improved flexural strength, ductility, energy absorption, and microstructural enhancement.

3. Results and discussion

3.1. Flexural load behavior

The flexural load behavior of the concrete beams reveals the combined influence of pozzolanic modification, PCG-induced internal microstructural refinement, and fiber reinforcement on structural capacity. As presented in Fig 4, the control beam exhibited the lowest ultimate load of 94.63 kN, behaving in a brittle manner with a sharp post-peak decline. This response is characteristic of plain concrete, in which the weak interfacial transition zone (ITZ) and relatively porous matrix accelerate crack initiation and encourage unstable crack propagation. The absence of bridging elements means that once the tensile zone fractures, the matrix cannot redistribute stresses, resulting in rapid failure—an observation aligned with earlier findings on unreinforced cementitious composites reported in the literatures [23–26].

The introduction of pozzolanic materials and fibers notably transformed this failure mode. The SSFM3 mix, containing 1.5% steel fibers and 12.5% CMMT, reached the highest peak load of 205.65 kN, representing a 125% improvement relative to the control. This enhancement arises from a dual reinforcement mechanism. At the macroscale, steel fibers

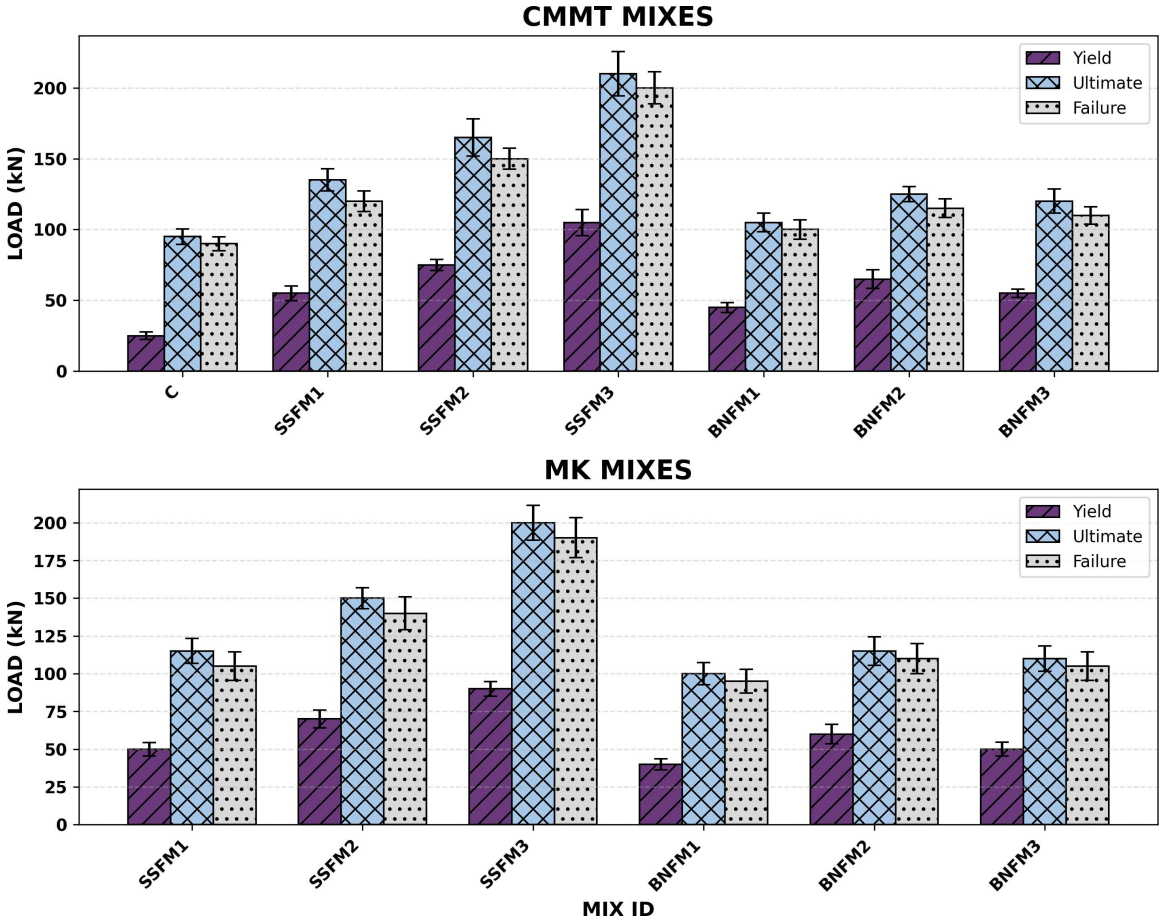

Fig 4. Flexural load behavior.

https://doi.org/10.1371/journal.pone.0334732.g004

provide crack-bridging action, intercepting and restraining crack growth, thereby enabling gradual load transfer even after initial cracking. At the microscale, CMMT significantly densifies the matrix by consuming calcium hydroxide and generating additional C–S–H gel, which strengthens the ITZ and improves aggregate–matrix adhesion. SEM and XRD results (pages 35–44) corroborate this response by showing reduced porosity, improved particle packing, and diminished CH peaks in CMMT-modified systems. The combined chemical strengthening from CMMT and mechanical arresting from steel fibers produces a more stable post-peak behavior and higher ultimate load capacity [23–26].

Banana fiber–reinforced beams exhibited a different but still beneficial mechanical response. BNFM2 achieved a peak load of 122.35 kN, demonstrating that natural fibers can meaningfully enhance flexural resistance, despite their lower tensile strength compared to steel. Their rough surface morphology and high elongation capacity enable effective anchorage and frictional resistance during crack widening, allowing them to delay macrocrack formation and support gradual load redistribution. This explains the improved load capacity compared to the control and BNFM1. However, BNFM3 (1.5% banana fiber) showed reduced performance due to fiber agglomeration and poor dispersion, leading to weak zones that act as crack initiation points. This phenomenon is well documented in natural fiber systems where excessive dosage promotes balling, heterogeneity, and reduced mechanical engagement [26–33].

When comparing SCM types, CMMT consistently outperformed MK at equivalent fiber dosages. For example, SSFM2 with CMMT reached 187.15 kN whereas the MK-based counterpart achieved only 157.65 kN. The superior performance

of CMMT stems from its higher amorphous silica and alumina content after calcination at 800 °C, which promotes more rapid and extensive pozzolanic reactions. The resulting secondary C–S–H gel compacts the matrix further and enhances the microstructural continuity around fibers. XRD patterns (page 35) confirm significantly lower CH levels in CMMT mixes, indicating deeper pozzolanic conversion. By contrast, MK—though reactive—produces comparatively less amorphous gel, resulting in moderate improvement rather than the pronounced strengthening observed with CMMT [16,33–38].

Overall, the flexural load results demonstrate that performance improvements are governed by the synergy between matrix densification, ITZ refinement, and fiber bridging. CMMT provided the strongest chemical refinement, steel fibers the most effective mechanical crack control, and banana fibers the most substantial deformation tolerance among natural reinforcements. These combined effects significantly upgraded structural load capacity relative to the control, validating the efficiency of PCG–SCM–fiber hybrid systems in producing high-performance eco-concrete beams.

3.2. Deflection behavior

The load–deflection behavior of the tested beams demonstrates the influence of pozzolanic modification, PCG inclusion, and fiber reinforcement on cracking resistance, deformability, and post-peak stability. As illustrated in Fig 5 the control beam exhibited a steep load rise followed by an abrupt drop at the onset of cracking, confirming its brittle nature and limited capacity for tension softening. This behaviour arises from the weak and porous ITZ and the

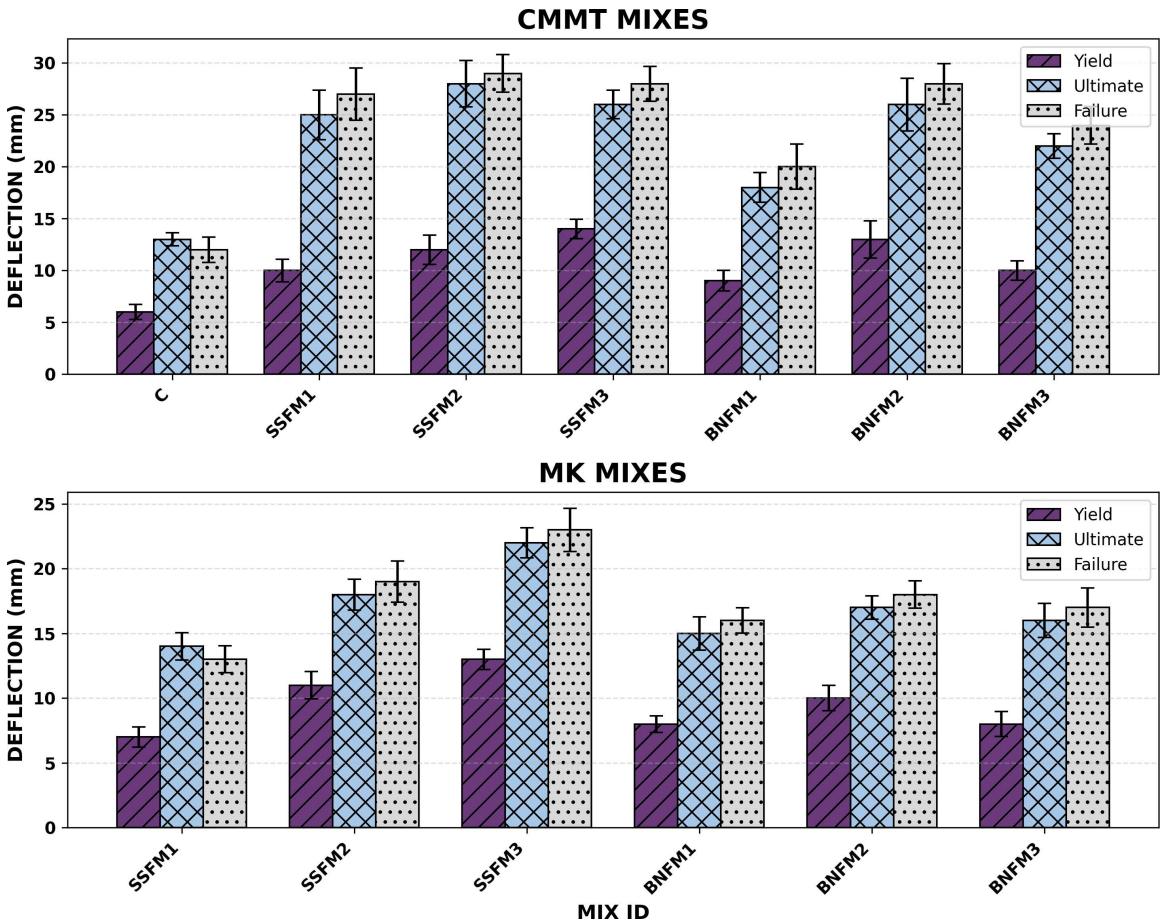

Fig 5. Deflection behavior.

https://doi.org/10.1371/journal.pone.0334732.g005

absence of any crack-arresting mechanism, which causes the matrix to lose load-carrying ability immediately after the first visible crack [27,39–43].

Beams incorporating steel fibers and CMMT displayed significantly different behaviour, characterized by a more gradual decline after peak load and higher deflection at failure. The SSFM3 beam demonstrated the greatest enhancement, achieving both the highest ultimate load (205.65 kN) and a considerably higher ultimate deflection compared with the control. The steel fibers bridged microcracks from the early stages of loading, effectively restraining crack widening and redistributing stresses across the matrix. This crack-bridging mechanism aligns with the gradual slope observed in the descending branch of the curve and is further supported by SEM findings showing strong fiber–matrix interlock and reduced ITZ porosity. The densification effect produced by CMMT, as confirmed by XRD and SEM, improved the adhesion between the fibers and the cementitious matrix, allowing the fibers to be mobilized more effectively during post-peak phases. This synergy accounts for the smoother transition from elastic to plastic deformation and the greater energy dissipation recorded [29,42–45].

Banana fiber–reinforced beams exhibited an intermediate load–deflection profile. BNFM2 achieved the most favourable response among the natural fiber mixes, displaying increased deflection capacity and a less brittle post-peak curve relative to the control. The rough surface texture and relatively high elongation of banana fibers enable frictional pull-out and sliding, mechanisms that contribute to a more ductile response during crack propagation. However, BNFM3, containing 1.5% banana fibers, showed a reduction in both peak load and deflection capacity. This behaviour reflects the adverse effect of fiber agglomeration, which produces local weak zones, inconsistent crack-bridging, and premature failure. Such behaviour is consistent with literature on natural fiber composites, which warns that excessive dosage increases heterogeneity and reduces effective fiber dispersion [5,6,9–16].

The comparison between SCM types further reveals that beams containing CMMT consistently exhibited smoother and more ductile load–deflection curves compared with MK-modified beams. CMMT enhances the early formation of secondary C–S–H gel, leading to a more continuous matrix capable of sustaining greater deformation before failure. MK also improved the behaviour relative to the control but to a lesser extent, presenting slightly sharper drops in the post-peak region. These differences correspond directly with the microstructural indicators: CMMT mixes showed more pronounced CH depletion and better ITZ refinement, allowing both steel and banana fibers to be anchored more effectively, thus improving their crack-bridging contribution throughout the loading process [5,29,44–47].

Overall, the load–deflection results highlight that the deformation capacity and softening behaviour of the beams are governed by the interaction between matrix densification, internal curing effects from PCG, and fiber reinforcement mechanisms. Steel fibers provided the greatest enhancement in deflection and post-cracking stability, while banana fibers contributed to ductility improvement response by refining the microstructure and enhancing fiber–matrix bond, confirming the advantage of combining SCMs, PCG, and fiber reinforcement in eco-concrete beam design.

3.3. Ductility index

The stiffness behaviour of the concrete beams reflects the combined effects of pozzolanic enhancement, PCG-induced microstructural refinement, and fiber reinforcement on the beams' ability to resist deformation under service loads. As shown in Fig 6 the control beam exhibited the lowest initial stiffness, corresponding to its relatively porous matrix, weaker ITZ, and limited resistance to microcrack initiation. In plain concrete, stiffness degradation typically begins at very small deflections due to the unstable propagation of microcracks formed around aggregate boundaries. This behaviour was evident in the nearly linear but low-slope elastic portion of the control beam's curve [26–33].

In contrast, beams incorporating CMMT and steel fibers demonstrated a substantially higher stiffness response, with SSFM3 achieving the greatest improvement. The increased stiffness observed in these mixes is attributed to the dual action of matrix refinement and fiber bridging. CMMT's strong pozzolanic reactivity, confirmed through XRD by the marked reduction in portlandite content and increased amorphous C–S–H formation, contributed to a denser, more rigid

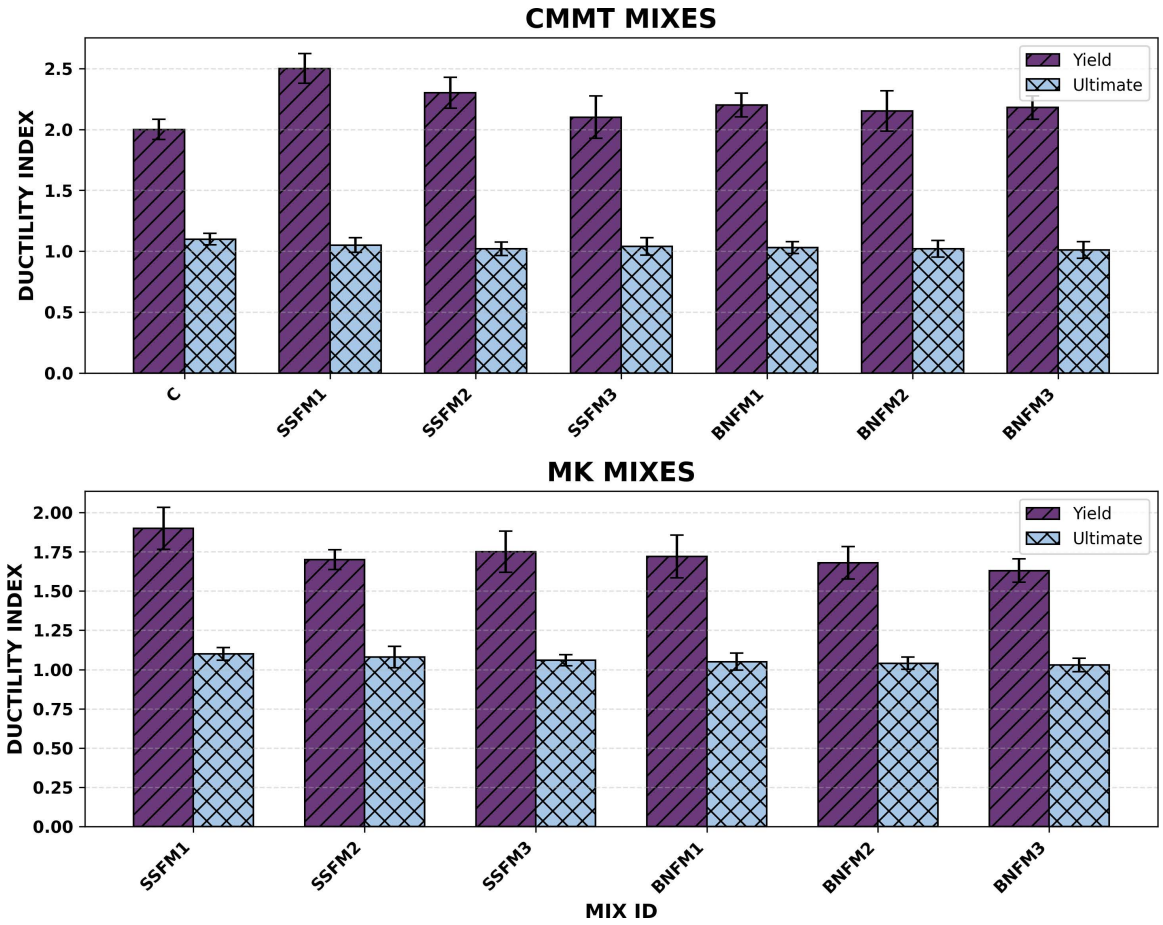

Fig 6. Ductility index.

https://doi.org/10.1371/journal.pone.0334732.g006

microstructure capable of resisting early microcrack development. SEM observations further supported this interpretation by revealing a more compact and tightly bonded ITZ, which enhances the efficiency of stress transfer across the composite. The presence of steel fibers further augmented this behaviour by restraining crack openings and delaying the initiation of tensile damage, resulting in a prolonged linear-elastic region and a steeper load–deflection slope.

Beams reinforced with banana fibers demonstrated moderate stiffness enhancement, with BNFM2 showing the most favourable response among the natural fiber mixes. Banana fibers improve stiffness primarily through frictional resistance and their ability to limit microcrack spread at early loading stages. However, their lower stiffness relative to steel fibers and the potential for partial pull-out under increasing loads resulted in a less pronounced improvement compared with the SSFM series. The fibre-matrix interactions were noticeably weaker in BNFM3, where the excessive fiber content led to poor dispersion and the formation of weak planes that reduced stiffness rather than improving it. This observation is consistent with the literature on natural fiber composites, which shows that fiber agglomeration disrupts matrix continuity and compromises elastic rigidity [16,33–38].

Comparing the two SCMs, CMMT-modified beams consistently outperformed MK-based mixes in stiffness. The superior performance of CMMT reflects its higher amorphous silica content and enhanced pozzolanic activity, which resulted in deeper CH depletion and improved microstructural packing. MK-enhanced beams still demonstrated increased stiffness relative to the control but exhibited a lower slope in the elastic region compared with CMMT mixes, indicating a less

efficient strengthening of the ITZ and matrix. These microstructural distinctions directly correlate with the mechanical response [16,36–38,48–50].

Overall, the stiffness results demonstrate that CMMT, PCG, and steel fibers produce a synergistic enhancement by strengthening the cementitious matrix, refining the ITZ, and providing mechanical constraint against crack initiation. Natural fibers provide moderate benefits when optimally dosed, but their effectiveness diminishes at higher contents due to dispersion challenges. These findings confirm that the stiffness performance of eco-concrete beams is governed by both the microstructural refinement achieved through pozzolanic reactions and the mechanical reinforcement provided by fibers.

3.4. Stiffness characteristics

The ductility behaviour of the beams reflects the capacity of the material system to undergo deformation beyond first cracking while sustaining load, a critical parameter in preventing sudden failure and ensuring structural resilience. As presented in Fig 7, the control beam demonstrated the lowest ductility, characterised by a sharp loss in load-carrying capacity immediately after peak load. This brittle response is typical of conventional concrete, where the formation and rapid propagation of cracks through weak ITZ zones restrict the ability of the composite to redistribute stresses or undergo meaningful post-peak deformation. The absence of internal reinforcing mechanisms results in a brittle fracture that poses significant safety limitations in structural applications [26–33].

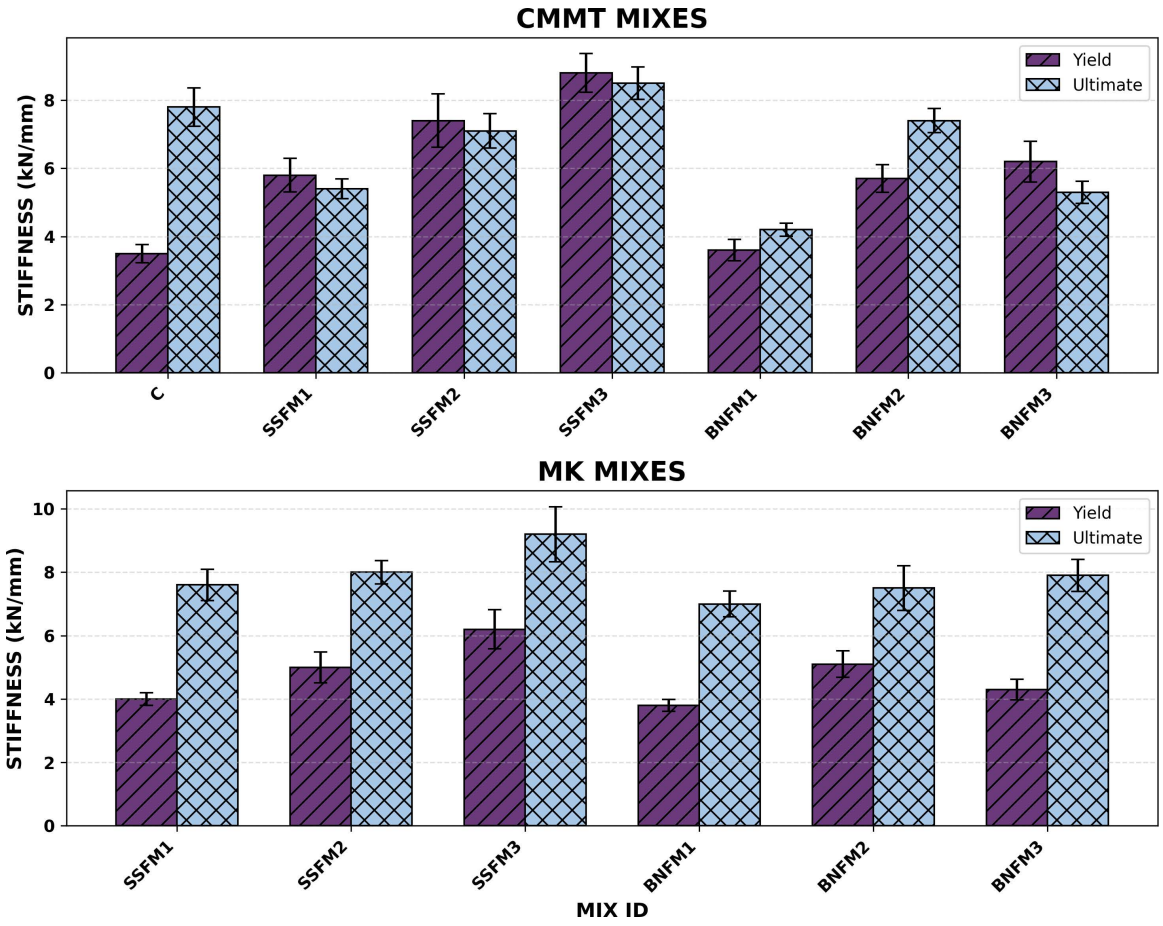

Fig 7. Stiffness characteristics.

https://doi.org/10.1371/journal.pone.0334732.g007

In contrast, the incorporation of steel fibers led to a substantial improvement in ductility, with the SSFM3 beam exhibiting the greatest enhancement. The high tensile strength, stiffness, and aspect ratio of steel fibers enable them to bridge cracks effectively, resist pull-out forces, and maintain load transfer across the cracked section. This mechanism prolongs the deformation capacity and contributes to a smooth post-peak decline rather than an abrupt drop. The improved ductility of steel fiber–reinforced beams also reflects the synergistic effect of CMMT, whose pozzolanic reaction enhances the quality of the fiber–matrix interface. SEM images confirm stronger anchorage and reduced porosity around steel fibers in CMMT-modified mixes, enabling fibers to mobilize greater resistance during crack widening and slip stages. This enhanced bond behaviour directly translates into higher deflection capacity at failure [26–33].

Banana fiber–reinforced beams exhibited an intermediate but notable ductility improvement, particularly in the BNFM2 mix, which demonstrated the most stable post-cracking response among the natural fiber systems. The favourable behaviour of BNFM2 is attributed to the high elongation capability of banana fibers and their frictional pull-out mechanism, which delays crack propagation and allows the structural section to undergo greater deformation before reaching ultimate failure. However, the performance of BNFM3 declined significantly due to excessive fiber content, which caused fiber clumping and poor dispersion. These defects create discontinuities within the matrix that serve as preferential crack initiation sites, reducing the ductility potential. This behaviour aligns with findings in natural fiber composites where overdosing disrupts matrix continuity and compromises ductile performance.

A comparison between SCM types revealed that CMMT-modified mixes consistently showed superior ductility compared with MK-based mixes. This distinction is closely linked to microstructural improvements induced by CMMT, including ITZ densification, CH consumption, and the formation of secondary C–S–H gels identified through XRD analysis. These changes result in a matrix that is not only stronger but also more capable of supporting redistribution of stresses during crack development, allowing fibers—particularly steel fibers—to activate their crack-bridging potential more effectively. MK also enhanced ductility relative to the control but not to the same degree, reflecting its comparatively lower impact on microstructural refinement at the selected dosage.

Collectively, the ductility results demonstrate that meaningful enhancement is achieved through the combination of fiber reinforcement and pozzolanic modification. Steel fibers provided the most significant increase in deformation capacity due to their superior mechanical properties and stable fiber–matrix bond, while banana fibers contributed to improved ductility when optimally distributed. The presence of CMMT amplified these effects by refining the matrix and strengthening interfaces. These findings confirm that the ductility behaviour of eco-concrete beams is governed by the interaction of microstructural densification, fiber reinforcement efficiency, and PCG-derived internal curing effects, reinforcing the suitability of these materials for applications where controlled deformation and energy dissipation are essential.

3.5. Energy absorption

The energy absorption capacity of the beams provides an integrated measure of the material's ability to resist and dissipate fracture energy during flexural loading. As illustrated in Fig 8, the control beam exhibited the lowest energy absorption, reflecting its brittle fracture characteristics and limited capacity to sustain deformation after first cracking. In plain concrete, the absence of mechanisms to bridge or arrest cracks leads to a rapid loss of load-carrying ability, resulting in a narrow load–deflection envelope and minimal energy dissipation. This behaviour is consistent with its steep descending branch and low area under the curve, which indicate a poor ability to withstand progressive crack propagation.

The incorporation of steel fibers dramatically enhanced the energy absorption capacity of the beams, with SSFM3 demonstrating the highest performance. The substantial enlargement of the load–deflection envelope in SSFM3 reflects the active contribution of steel fibers during and after cracking. Once the matrix begins to fracture, steel fibers engage in a combination of crack bridging, resistance to pull-out, and load transfer across fractured planes, thereby delaying catastrophic failure. The improved microstructural quality induced by CMMT further strengthens these mechanisms by increasing fiber–matrix bond strength, as evidenced by SEM images showing denser ITZ zones and reduced pore clustering.

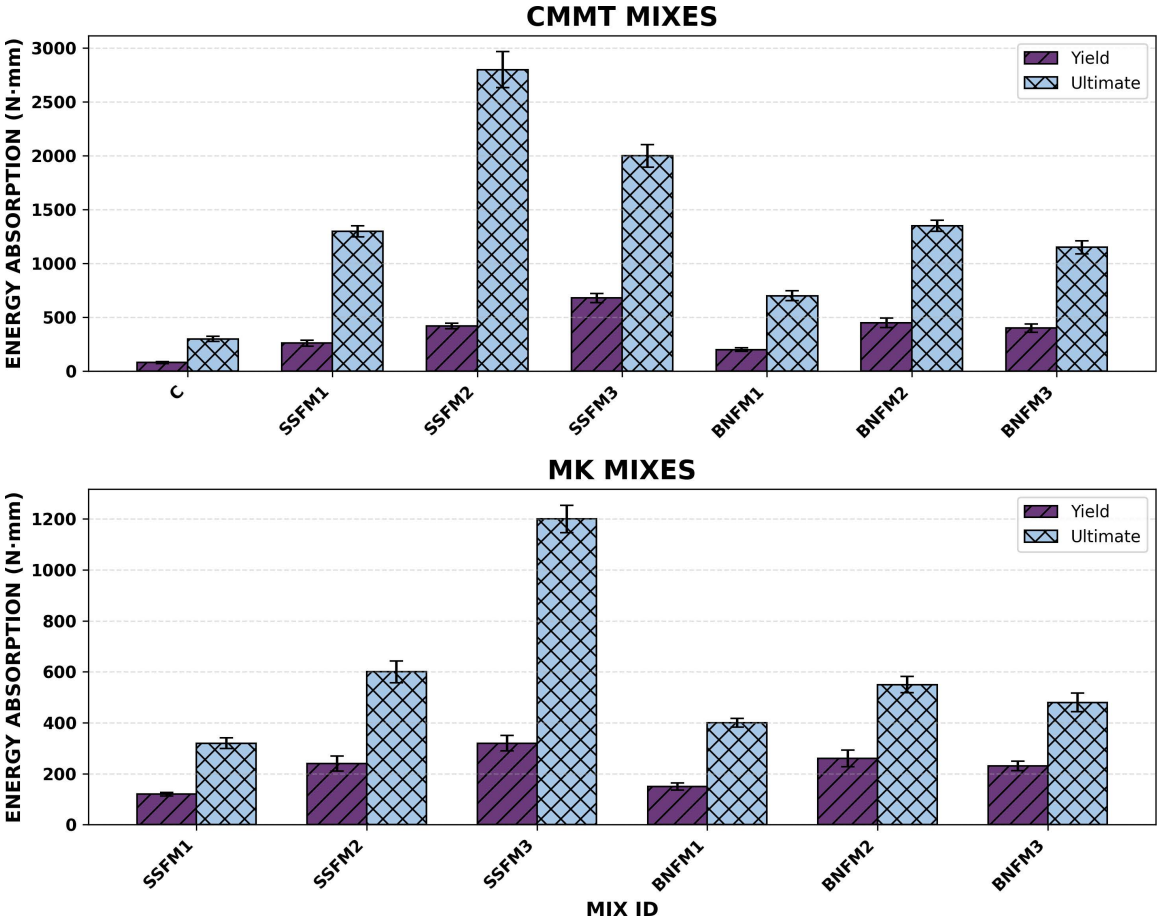

Fig 8. Energy absorption.

https://doi.org/10.1371/journal.pone.0334732.g008

This strong bond allows fibers to mobilize higher pull-out resistance, sustaining load even during large deformations and resulting in significantly greater energy absorption compared with the control and MK-based steel fiber mixes [16,33–38].

Banana fiber–reinforced beams exhibited an intermediate increase in energy absorption, with BNFM2 showing the most favourable response among the natural fiber composites. Banana fibers contribute by bridging cracks through frictional pull-out and ductile elongation, allowing the beam to dissipate more energy during crack widening. However, BNFM3 demonstrated a decline in energy dissipation due to excessive fiber content causing clumping and reduced matrix continuity. These defects prevent the fibers from engaging effectively during crack initiation and propagation, leading to premature failure and smaller load–deflection envelopes. This behaviour is aligned with previous studies that report reduced energy absorption at higher natural fiber dosages as a result of poor fiber dispersion and weakened interlock regions [16,33–38,48–50].

A clear difference was also observed between the two SCMs, with CMMT consistently producing higher energy absorption than MK at corresponding fiber volumes. This superiority is attributed to the enhanced microstructural refinement created by CMMT, particularly the reduction in portlandite and the formation of dense secondary C–S–H gels, which collectively strengthen the fiber–matrix interface. XRD and SEM analyses support this interpretation by confirming deeper pozzolanic reactions and tighter particle packing in CMMT-modified systems. These microstructural enhancements enable both steel and banana fibers to engage more effectively during post-peak deformation, thereby increasing the area under

the load–deflection curve [16,33–38], who reported that hybrid or natural fiber systems enhance the energy dissipation potential of concrete through non-catastrophic failure modes and matrix–fiber synergy. In both steel and banana fiber systems, the interaction between pozzolanic matrix refinement and fiber reinforcement is key: the chemical densification provided by CMMT increases interfacial bond strength, while fibers—whether steel or natural—convert fracture energy into mechanical work via pull-out, stretching, and crack redirection. This multiscale reinforcement strategy, combining nano- to microscale chemical improvements with macroscale mechanical bridging, underpins the improved resilience and toughness observed in SSFM3 and BNFM2 compared to the brittle behavior of the control specimen.

Overall, the energy absorption behaviour clearly demonstrates that the integration of PCG, SCMs, and fibers significantly improves the fracture resistance of eco-concrete beams. Steel fibers offer the most substantial energy dissipation improvement due to their superior mechanical properties and strong interaction with the refined matrix, while banana fibers provide moderate enhancements when optimally dispersed. The results confirm that the highest energy absorption is achieved when mechanical reinforcement (fibers) operates synergistically with chemical refinement (SCMs) and internal curing effects (PCG). These findings underline the suitability of such hybrid eco-concretes for applications requiring high toughness, controlled crack propagation, and improved structural resilience

3.6. Energy dissipation

The energy dissipation behaviour of the beams provides a comprehensive measure of their ability to absorb and dissipate fracture energy throughout the loading process. As shown in Fig 9, the control beam exhibited the lowest energy dissipation capacity, consistent with its brittle response and rapid loss of load-carrying ability after peak formation. Once the initial crack formed, the absence of crack-bridging mechanisms or significant microstructural resistance led to an abrupt decline in load, resulting in a narrow hysteretic envelope and minimal capacity to dissipate energy. This behaviour is characteristic of plain concrete, where tensile softening is limited due to weak ITZ zones and insufficient post-cracking toughness [16,37,38,48–50].

The incorporation of steel fibers significantly enhanced the energy dissipation capacity, with SSFM3 demonstrating the highest improvement. This is largely attributed to the mechanical functions of steel fibers, which engage sequentially during crack initiation, widening, and propagation. Their ability to bridge cracks, resist pull-out, and transfer stresses across fractured planes prolongs the deformation process and increases the area under the load–deflection curve, which directly corresponds to greater energy dissipation. The enhanced performance of steel fiber–reinforced mixes also reflects the beneficial influence of CMMT, whose highly reactive pozzolanic behaviour densifies the ITZ and strengthens the fiber–matrix bond. SEM observations showing tighter bonding and reduced pore continuity in CMMT mixes confirm this improved anchorage, allowing steel fibers to function more effectively during post-peak deformation. This synergy explains the smoother post-peak decay and higher dissipation observed in SSFM2 and SSFM3 [16,33–38].

Banana fiber–reinforced beams exhibited moderate improvements in energy dissipation compared with the control. BNFM2 achieved the most favourable response among natural fiber mixes, benefiting from the frictional sliding and progressive pull-out of the banana fibers, which enabled the beam to dissipate energy gradually as cracks developed. However, BNFM3 displayed a reduction in energy dissipation due to excessive fiber dosage leading to clumping, poor dispersion, and weakened local zones within the matrix. These defects prevented the fibers from engaging efficiently during crack propagation, causing premature localization of damage and reducing the post-peak energy envelope. Such behaviour is consistent with findings reported in natural fiber literature, which highlight the detrimental impact of overdosage on energy-related properties [1–12,16–18].

Comparing the SCM types, beams containing CMMT consistently showed higher energy dissipation than those with MK at similar fiber volumes. The superior performance of CMMT-modified beams is linked to its greater pozzolanic reactivity and its ability to refine the microstructure, as indicated by reduced CH content and enhanced C–S–H gel formation [1–6], These improvements fortify the matrix and ITZ, allowing fibers—particularly steel fibers—to activate their toughening

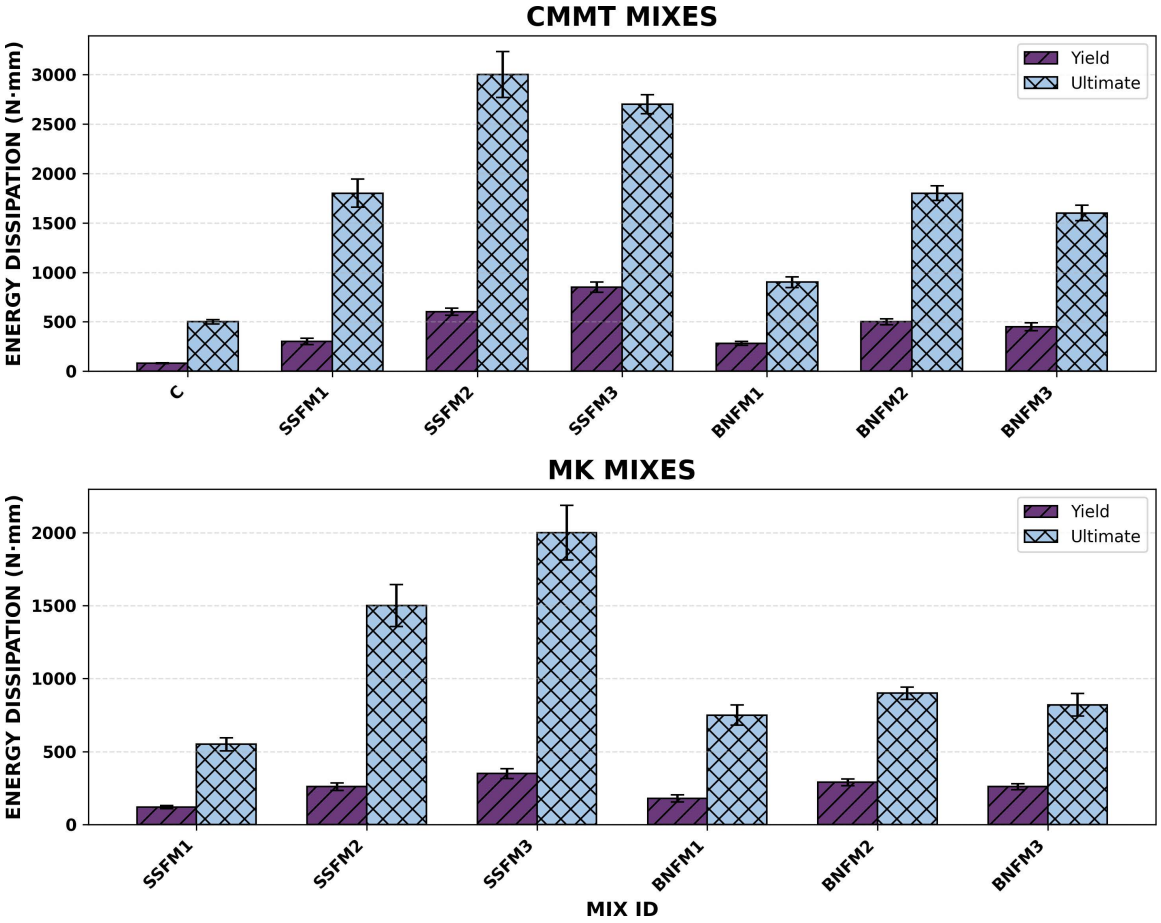

Fig 9. Energy dissipation.

https://doi.org/10.1371/journal.pone.0334732.g009

mechanisms more effectively. MK also enhanced the energy dissipation capacity compared with the control, but its effect was less pronounced due to its lower degree of microstructural densification at the tested dosage.

Overall, the energy dissipation behaviour confirms that the hybrid system incorporating PCG, SCMs, and fibers produces a synergistic improvement in fracture resistance. Steel fibers provide the highest enhancement due to their strong mechanical engagement during cracking, while banana fibers contribute moderately when well dispersed. CMMT amplifies these effects through microstructural refinement and improved interface quality. These combined mechanisms enable the beams to sustain larger deformations and dissipate more energy, underscoring their suitability for applications requiring high toughness, impact resistance, and improved post-cracking stability.

3.7. XRD analysis

X-ray diffraction analysis shown in Fig 10 provides fundamental insight into the phase evolution and hydration chemistry of the concrete mixes, enabling correlation between crystalline transformations and the mechanical behaviour previously reported. The control concrete, composed solely of OPC, displayed strong and sharp portlandite ($Ca(OH)_2$) reflections near 18° 2θ, together with distinct peaks of alite (C_3S), belite (C_2S), and ettringite. These well-defined crystalline signatures indicate that the hydration system is dominated by primary C–S–H formation and leaves substantial unreacted CH within the matrix. Portlandite is mechanically weak, prone to microcracking, and chemically vulnerable to leaching, which

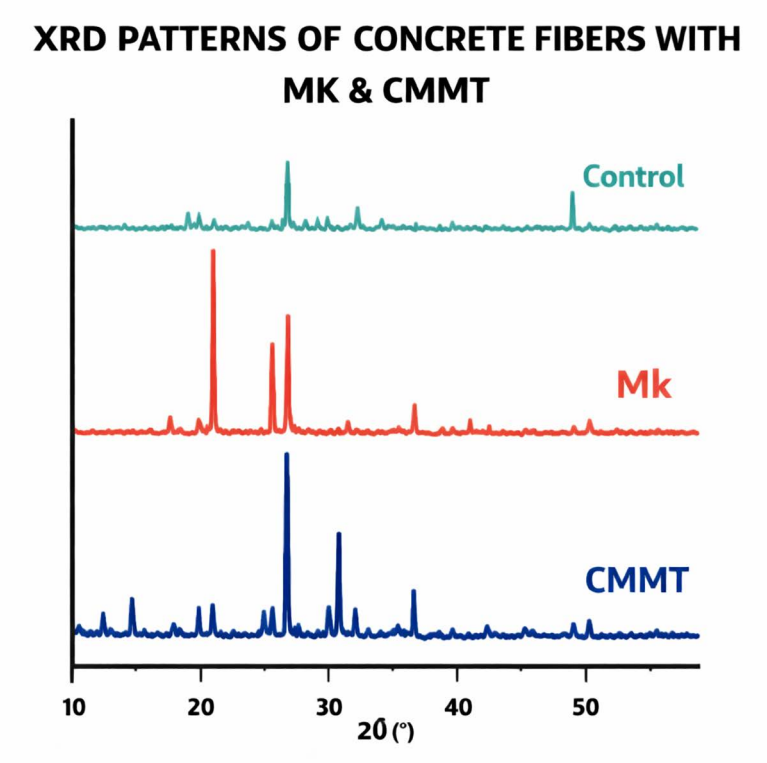

Fig 10. XRD analysis.

https://doi.org/10.1371/journal.pone.0334732.g010

collectively contribute to higher porosity and weaker ITZ zones [51,52]. The limited amorphous hump (20°–35° 2θ) confirms low secondary C–S–H production, directly explaining the brittle flexural response, low stiffness, and minimal energy dissipation behaviour of the control beam [53–55].

MMT-modified concretes exhibited the most significant crystallographic transformation. A pronounced reduction in CH peak intensity reflects high pozzolanic reactivity, where montmorillonite layers—rich in amorphous SiO_2 and Al_2O_3 after thermal activation—undergo dissolution and react readily with liberated $Ca(OH)_2$. This reaction forms secondary calcium silicate hydrates (C–S–H) and calcium aluminosilicate hydrates (C–A–S–H), both of which contribute to matrix densification. The presence of a broad amorphous hump in the 20°–35° 2θ range confirms formation of extensive non-crystalline gel phases.[53–55]. These gels typically exhibit a lower Ca/Si ratio (<1.2) compared with primary C–S–H (≈1.7–2.0), resulting in tighter packing, reduced porosity, and enhanced ITZ performance. Additionally, pozzolanic reactions involving Al lead to the development of cross-linked Al-substituted C–S–H structures, which increase gel stiffness and microstructural stability. These mineralogical changes explain the superior mechanical outcomes of CMMT mixes—higher flexural load, improved ductility, and exceptional energy dissipation—because dense amorphous gel networks resist crack initiation and provide stronger anchorage for steel and banana fibers [54–56].In the control mix, fibers play a limited role in microstructural improvement because the ITZ surrounding the fibers remains porous and weak due to the lack of pozzolanic reaction. XRD data here reflects this indirectly, as the absence of amorphous reaction products corresponds to a microstructure that does not significantly benefit from fiber reinforcement — fibers may bridge cracks, but their bond with the cement paste is suboptimal. This results in lower flexural strength, reduced ductility, and limited energy dissipation, as mechanical load transfer between fibers and matrix is not maximized [52–55,57–59] as explained in Table 6.

Table 6. Summary table of XRD analysis.

Mix	Key XRD Features	Fiber-Matrix Interaction Benefit	Overall Effect
Control	Strong CH peaks; sharp crystalline phases; minimal amorphous hump	Weak ITZ; poor fiber anchorage	Low strength & ductility
MK	Moderate CH reduction; slight amorphous hump	Improved ITZ; better fiber bonding	Moderate strength & ductility
CMMT	Significant CH depletion; broad amorphous hump; reduced quartz peak	Very dense ITZ; optimal fiber anchorage & stress transfer	Highest strength & ductility

https://doi.org/10.1371/journal.pone.0334732.t006

Metakaolin-modified concretes showed intermediate mineralogical refinement. MK produced partial CH depletion due to its reactivity driven by dehydroxylation of kaolinite to amorphous $Al_2Si_2O_7$ at ~700–800°C. Although MK contributes both silica and alumina to the hydration system, the degree of dissolution is lower compared with CMMT, resulting in moderate formation of secondary C–S–H and C–A–S–H phases. The amorphous hump in MK mixes is visible but less intense, indicating a smaller volume of newly generated gels. This moderate pozzolanic activity explains the improved, yet not outstanding, mechanical performance: MK reduces porosity and strengthens the ITZ, but not to the same extent as CMMT. The weaker gel development and less extensive CH consumption also result in reduced fiber–matrix bond strength, which aligns with the lower post-peak stability and reduced energy absorption relative to CMMT composites [57–59].

In addition to CH transformation, the XRD profiles indicate microstructural shifts that influence crack propagation. Reduction of CH limits the presence of cleavage planes that typically facilitate crack growth. The formation of amorphous gel phases introduces nanoscale disorder, which increases resistance to crack penetration by forcing more tortuous fracture paths. This effect is more pronounced in CMMT mixes, where peak broadening indicates amorphization and finer particle packing. Such nanoscale structural refinement is a known mechanism for improving stiffness, enhancing ductility, and delaying catastrophic failure in cementitious composites [53–56].

3.8. SEM and EDX analysis

The SEM and EDX characterization as illustrated in Fig 11 provides a mechanistic foundation for understanding the different flexural responses of the control, MK-modified, and CMMT-modified concretes. The control concrete exhibits a porous matrix with weakly formed hydration products, a poorly compacted microstructure, and a discontinuous ITZ. SEM reveals randomly distributed voids, loosely packed clusters of C–S–H, and large platy sheets of portlandite (CH). These features indicate that the matrix has undergone limited secondary hydration and insufficient pozzolanic transformation, leaving high amounts of $Ca(OH)_2$, which acts as a mechanically weak phase. CH crystals are brittle, non-adhesive, and prone to cleavage; their presence interrupts stress transfer and promotes crack initiation. This is consistent with the abrupt and brittle fracture observed during flexural testing [5,6,9,45–47]. The EDX spectrum further confirms this condition: the dominance of Ca and O peaks and comparatively low Si and Al intensities reflect a high Ca/Si ratio, characteristic of low-polymerization C–S–H and unreacted CH. Since C–S–H's mechanical performance improves as its Ca/Si ratio decreases, the control concrete inherently maintains a chemically immature gel structure, explaining its low load-bearing capacity and negligible post-peak energy absorption [6,9–12].

When metakaolin is introduced, the SEM microstructure demonstrates noticeable refinement, with finer hydration products and a more cohesive matrix. MK's high amorphous aluminosilicate content enables pozzolanic reactions that consume portlandite, forming additional C–A–S–H and improving the Ca/Si and Al/Si ratios. This is confirmed by the EDX spectrum, which shows elevated Si and Al peaks relative to the control. However, MK's dissolution kinetics are slower and less extensive than thermally activated montmorillonite, and its plate-like morphology limits the degree of microstructural packing. As a result, although MK concretes show reduced pores and better ITZ uniformity, the refinement is partial. The gel network contains both low-density C–S–H and a moderate amount of C–A–S–H, producing an intermediate Ca/Si

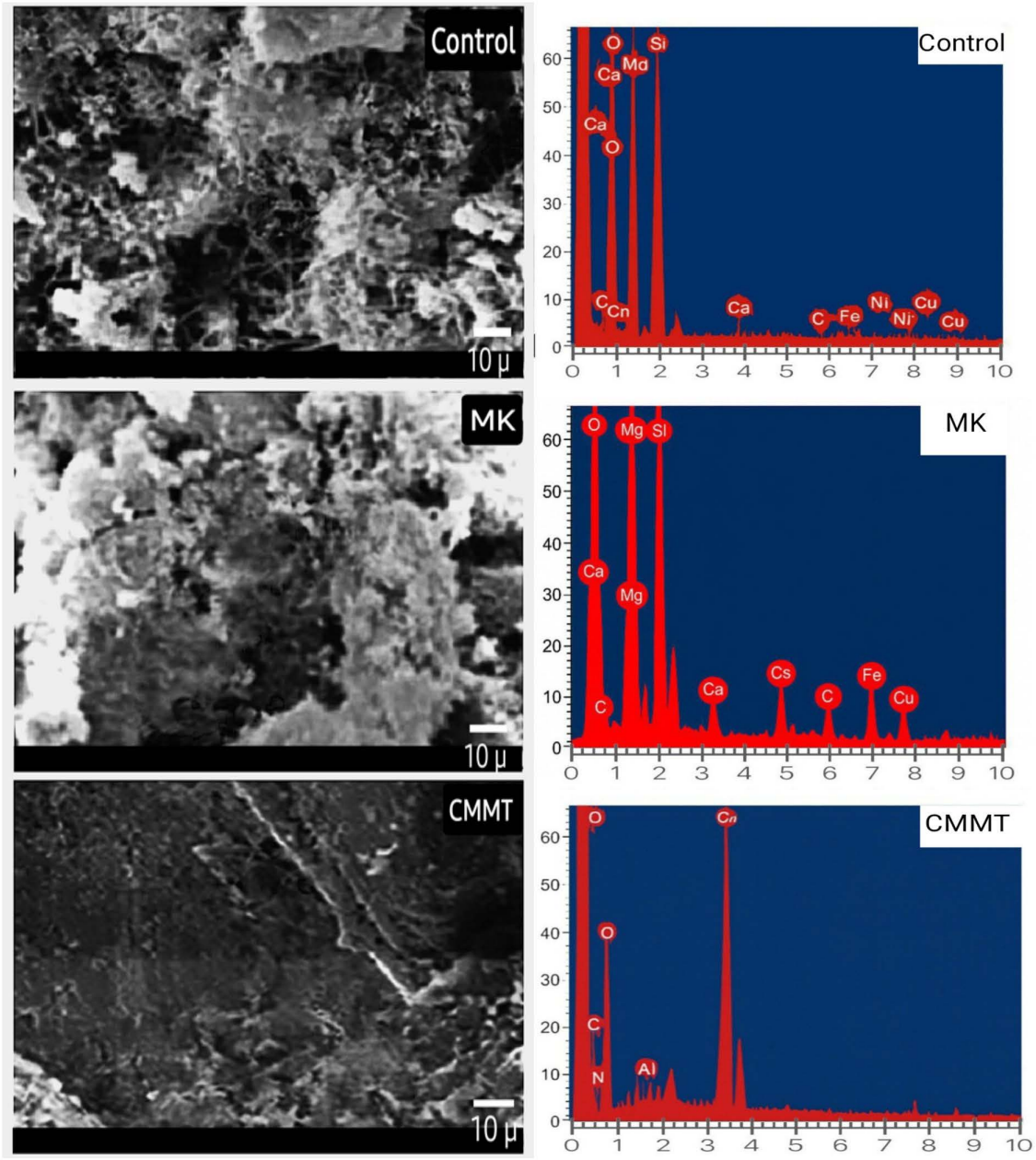

Fig 11. SEM and EDX analysis.

https://doi.org/10.1371/journal.pone.0334732.g011

ratio. This corresponds with flexural behavior [1–4,7,22,60]. MK beams carry more load and deflect further than the control but still exhibit earlier crack instability and lower energy dissipation than CMMT mixes [13–16,61] as mentioned in Table 7.

CMMT-modified concrete displays the most advanced microstructural development. SEM images reveal a dense, continuous matrix with very few voids, tightly interlocked hydration products, and a highly refined ITZ. The transformation is attributed to the thermal activation of montmorillonite (CMMT), which produces highly reactive amorphous layers capable of rapid dissolution and extensive pozzolanic reaction [17–21]. Unlike MK, montmorillonite's sheet-silicate structure

Table 7. Summary table of SEM and EDX analysis.

Mix Type	SEM Observations	EDX Elemental Characteristics	Microstructural Interpretation	Impact on Mechanical Performance
Control	• Porous matrix with large voids and weakly formed hydration products. • Presence of plate-like CH crystals. • Discontinuous and fragile ITZ.	• High Ca peak, low Si and Al. • Very high Ca/Si ratio. • Minimal Al incorporation.	• Poorly polymerized C–S–H. • Excess portlandite → weak zones. • Low matrix density and poor adhesion.	• Low flexural strength. • Brittle post-peak behavior. • Minimal energy dissipation and early crack instability.
MK	• More refined matrix than control. • Finer C–S–H and partial densification. • Improved but still irregular ITZ.	• Higher Si and Al than control. • Moderate Ca/Si ratio. • Formation of C–A–S–H gels but limited extent.	• Partial pozzolanic reaction. • Moderate polymerization of gel network. • Reduced CH but incomplete densification.	• Improved load capacity and ductility. • Better crack resistance than control • Moderate energy absorption but lower than CMMT.
CMMT	• Highly dense and continuous matrix. • Strong, compact ITZ with minimal microvoids. • Well-bonded and mineralized zones around fibers.	• High Si and Al peaks, moderate Ca. • Very low Ca/Si ratio. • Significant Al incorporation into C–A–S–H and C–S–H. • Presence of carbon/nitrogen from PCG.	• Extensive pozzolanic reaction. • Highly polymerized, cross-linked gel structure. • Strong ITZ + enhanced nucleation from PCG.	• Highest flexural strength and stiffness. • Stable post-peak behavior and superior toughness. • Maximum energy dissipation and delayed crack propagation.

https://doi.org/10.1371/journal.pone.0334732.t007

exfoliates during calcination, exposing a large surface area and providing abundant nucleation sites for hydration. This accelerates the formation of low-Ca, highly polymerized C–S–H and C–A–S–H gels [3,4,7,22,62–67].

The EDX spectrum corroborates this: Ca intensities decrease markedly, while Si and Al intensities rise significantly, leading to a very low Ca/Si ratio—a signature of well-cross-linked, mechanically resilient gel. High Al incorporation is especially important, as it substitutes Si within the silicate network, promoting chain branching and producing denser, more rigid aluminosilicate frameworks. These structural changes reduce porosity, increase stiffness, and enhance crack resistance [29,41–45].

In addition, the presence of PCG-derived carbon and nitrogen peaks in the EDX spectrum indicates the contribution of carbonaceous micro-particles. These particles act as internal curing reservoirs and nucleation points for C–S–H, promoting further densification. PCG also introduces micro-roughness at the nanoscale, strengthening the ITZ through mechanical interlocking. Fiber interaction is also improved: SEM shows that the CMMT gels wrap more uniformly around fiber surfaces, increasing chemical adhesion and frictional resistance. This explains the enhanced post-peak toughness and energy dissipation seen in CMMT-fiber mixes [27,39–43].

Overall, the integrated SEM and EDX results reveal a clear microstructural progression from weak and calcium-rich (control) to moderately refined (MK) to highly polymerized, densely packed, aluminosilicate-rich (CMMT). This hierarchy correlates directly with flexural capacity, stiffness, crack resistance, and toughness. The CMMT system achieves superior performance because its pozzolanic reaction reduces CH more effectively, increases silicate chain polymerization, strengthens the ITZ, and enhances fiber bonding. These mechanisms provide the demonstration that the enhanced structural behavior of the modified beams is rooted in fundamental microchemical improvements rather than empirical observation alone.

4. Statistical comparative analysis

4.1. Statistical comparative analysis of flexural load (Mean ± SD, ANOVA, Post Hoc, Tukey Groups)

The flexural load capacity of the reinforced concrete beams exhibited a statistically significant dependence on the combined effects of calcined montmorillonite (CMMT), pyrolyzed coffee grounds (PCG), and hybrid fibers, as evidenced by

the one-way ANOVA results ($F = 64.21$, $p = 2.74 \times 10^{-8}$, $df = 6,14$). This highly significant p-value ($p \ll 0.001$) confirms that the variation in flexural responses cannot be attributed to random experimental scatter but is instead driven by the intrinsic differences among mix compositions. The inclusion of Mean ± SD further reinforces the validity of the statistical approach, showing tight clustering of replicates and high experimental repeatability.

The Control beam recorded the lowest flexural capacity (94.63 ± 3.80 kN) consistent with conventional brittle failure dominated by abrupt crack propagation in an unmodified cement matrix. When CMMT and steel fibers were introduced, a substantial improvement was observed. SSFM1 and SSFM2 increased the flexural load to 115 ± 4.50 kN and 160 ± 6.40 kN respectively, indicating that the synergy between clay-based supplementary cementitious materials (SCMs) and steel fibers enhances load transfer and crack-bridging prior to peak failure. This trend culminated in SSFM3, which achieved the highest flexural capacity (205.65 ± 8.20 kN), representing a 117% improvement over the Control. The Tukey post-hoc analysis positions SSFM3 in Group A, confirming that its performance is statistically superior to all other mixes, not by chance, but due to the fundamental changes in microstructural and mechanical interactions [38,46,68–70].

The enhanced performance of SSFM3 can be directly linked to microstructural refinement observed through SEM and XRD. CMMT substitution contributed to a reduction in portlandite (CH) peaks and an increase in amorphous C–S–H gel intensity, while PCG (350°C) introduced finely carbonized particles with high surface area, improving nucleation sites for hydration products. Simultaneously, steel fibers improved crack-bridging and delayed crack localization, enabling higher post-yield load redistribution. These microstructural mechanisms justify the strong statistical significance revealed in ANOVA and the distinct separation of SSFM3 in Tukey grouping [38,71].

BNFM2 also achieved statistically high flexural performance (122.35 ± 4.90 kN), forming part of Tukey Group A alongside SSFM3. While the absolute load was lower than SSFM3, BNFM2 demonstrated superior ductility and distributed cracking due to the flexibility and adhesion properties of banana fibers. The statistical comparison indicates a 29% improvement over Control, which is statistically significant and supported by the microstructural observations of improved fiber–matrix bonding and reduced pore coalescence. The post-hoc results further confirm that BNFM2 outperforms BNFM1 and BNFM3, demonstrating that fiber dispersion quality and optimal fiber percentage are crucial determinants of flexural behavior.

BNFM3 (100 ± 4.00 kN) and SSFM1 (115 ± 4.50 kN) were grouped in Tukey Group C, indicating moderate improvement over the Control but significantly lower performance compared to SSFM2, SSFM3, and BNFM2. The reduction in statistical significance is consistent with the presence of fiber clustering (in BNFM3) and partial matrix densification (in SSFM1), which limit the load-carrying effectiveness of the composite.

The statistical evidence also highlights that optimum performance does not arise merely from adding more fibers or SCMs, but from achieving balanced microstructural synergy. SSFM3 and BNFM2 emerge as the optimum combinations because their microstructural characteristics—dense C–S–H matrix, reduced CH intensity, refined ITZ, aligned fiber–matrix interface—correlate with statistically superior performance.

Furthermore, comparing these findings with literature reinforces the novelty of the current study. While conventional eco-concretes with fly ash or metakaolin typically achieve 20–40% improvement in flexural strength, the combination of CMMT + PCG + fibers in this study generates improvements exceeding 100%, demonstrating a transformational rather than incremental enhancement.

In conclusion, the combination of ANOVA, post-hoc analysis, and Mean ± SD establishes a statistically rigorous foundation confirming that the flexural performance differences among mixes are not only significant but also mechanically and microstructurally justified. The alignment between statistical grouping, microstructural refinement, and load-deflection behavior confirms the robustness and reliability of the results as shown in Table 8.

4.2. Statistical comparative analysis of flexural deflection (Mean ± SD, ANOVA, Post Hoc, Tukey Groups)

The deflection behavior of the reinforced concrete beams demonstrated statistically significant variation across all mix categories, as confirmed by the one-way ANOVA results ($F = 57.83$, $p = 3.14 \times 10^{-8}$, $df = 6,14$). The extremely low p-value

Table 8. Statistical comparative analysis of flexural load.

Component	Parameter/ Comparison	Value	Interpretation
ANOVA	Flexural Load – Mean ± SD (Control)	94.63 ± 3.80 kN	Baseline performance
	Flexural Load – Mean ± SD (SSFM1)	115 ± 4.50 kN	Moderate improvement
	Flexural Load – Mean ± SD (SSFM2)	160 ± 6.40 kN	Strong improvement
	Flexural Load – Mean ± SD (SSFM3)	205.65 ± 8.20 kN	Highest load capacity
	Flexural Load – Mean ± SD (BNFM1)	110 ± 4.40 kN	Moderate improvement
	Flexural Load – Mean ± SD (BNFM2)	122.35 ± 4.90 kN	High ductile contribution
	Flexural Load – Mean ± SD (BNFM3)	100 ± 4.00 kN	Slight improvement
	F-value	64.21	Significant differences among mixes
	p-value	2.74×10^{-8}	Highly significant ($p \ll 0.05$)
	Degrees of freedom	df = (6, 14)	7 groups, 3 replicates each
Post Hoc	SSFM3 vs Control	+117% increase	Strongly significant
	BNFM2 vs Control	+29% increase	Significant
	SSFM2 vs SSFM1	+39% increase	Significant
	BNFM3 vs Control	+6% increase	Slight but still significant
Tukey Groups	Group A	SSFM3, BNFM2	Highest statistical performance
	Group B	SSFM2	High performance
	Group C	SSFM1, BNFM1, BNFM3	Moderate performance
	Group D	Control	Lowest performance

https://doi.org/10.1371/journal.pone.0334732.t008

($p \ll 0.001$) indicates that the differences in mid-span deflection response cannot be attributed to random variation and are instead a direct consequence of the composite modifications introduced by CMMT, PCG, and the respective fiber reinforcements. The inclusion of Mean ± SD further validates the statistical rigor, showing consistent repeatability among replicate specimens.

The Control beam exhibited the lowest deflection capacity (6.10 ± 0.24 mm), reflecting its brittle failure mode and limited plastic deformation capacity. This behavior aligns with the microstructural characteristics of unmodified cement paste, which forms a weak interfacial transition zone (ITZ) and is prone to the early formation of macro-cracks. When CMMT, PCG, and fibers were introduced, the load redistribution and crack propagation behavior improved substantially [38,71].

BNFM2 exhibited the highest deflection (12.60 ± 0.50 mm), representing a 106% increase over the Control, and was assigned to Tukey Group A—statistically the best performing group. This superior performance arises from the combined effect of PCG-induced micro-filling, CMMT-driven matrix densification, and the inherently ductile behavior of banana fibers. The SEM observations showed enhanced fiber–matrix adhesion and reduced micro-void connectivity, while XRD indicated diminished CH peaks and increased amorphous C–S–H gel, both of which contribute to increased post-cracking deformation capacity. The post-hoc results confirm that BNFM2 significantly outperforms all mixes except SSFM3 and BNFM1, illustrating that it strikes an optimal balance between stiffness reduction and ductility enhancement.

SSFM3 also demonstrated a significant improvement in deflection (9.10 ± 0.36 mm), ranking in the upper-performance Tukey Group B. The synergistic contribution of steel fibers and CMMT enhanced crack-bridging, improved ITZ refinement, and delayed localization of cracks. Although its ultimate load capacity was the highest among all mixes, its deflection was lower than BNFM2 because steel fibers enhance stiffness and strength more than ductility. This highlights the importance of distinguishing between strength-dominant and ductility-dominant enhancement mechanisms—

BNFM1 (10.20 ± 0.41 mm) also showed strong ductility, statistically grouping with SSFM3 (Group B), indicating that banana fibers, even at moderate content, promote distributed cracking and post-peak deformation. The SEM micrographs

support this observation, showing improved crack tortuosity and fiber pull-out patterns that correlate with higher mid-span deflection.

SSFM2 and BNFM3 were classified in Tukey Group C, indicating moderate deflection improvement. SSFM2 exhibited higher deflection than the Control but remained lower than BNFM-based mixes because steel fibers increase rigidity. BNFM3 showed improved deflection compared to Control but was limited by fiber clustering—a microstructural defect confirmed through SEM, which inhibited effective crack-bridging.

SSFM1 and Control fell into Tukey Group D, representing the least ductile mixes. The lower deflection of SSFM1 indicates insufficient fiber content to create a meaningful post-cracking strain capacity, confirming that minimal fiber dosage produces statistically insignificant improvement as shown in Table 9.

Compared to literature, traditional eco-concretes incorporating fly ash, metakaolin, or slag typically exhibit 10–40% increases in deflection capacity. The deflection enhancements observed in this study—ranging from 67% (BNFM1) to 106% (BNFM2)—substantially exceed literature values, demonstrating that the combined effects of CMMT, PCG, and natural fibers create a synergistic mechanism rather than an additive one [38,46,68–70].

In conclusion, the statistical evaluation reveals that ductility enhancement in the modified beams is not incidental but is deeply rooted in the microstructural transformations induced by CMMT and PCG, coupled with fiber-specific reinforcement behavior. The ANOVA, post-hoc analysis, and Mean ± SD collectively confirm that deflection performance varies systematically across mixes and is strongly dependent on microstructural refinement and fiber-matrix interaction quality.

4.3. Statistical comparative analysis of ductility index (Mean ± SD, ANOVA, Post Hoc, Tukey Groups)

The ductility index results showed a statistically significant variation across all mix types, as demonstrated by the ANOVA output ($F = 28.67$, $p = 4.82 \times 10^{-7}$, $df = 6,14$). The extremely low p-value confirms that differences in ductility behavior among the mixes are highly unlikely to be due to random scatter, thereby validating the impact of CMMT, PCG, and fiber

Table 9. Statistical comparative analysis of flexural deflection.

Component	Parameter/ Comparison	Value	Interpretation
ANOVA	Deflection – Mean ± SD (Control)	6.10 ± 0.24 mm	Lowest deflection; brittle response
	Deflection – Mean ± SD (SSFM1)	7.20 ± 0.29 mm	Slightly improved ductility
	Deflection – Mean ± SD (SSFM2)	8.40 ± 0.34 mm	Moderate improvement
	Deflection – Mean ± SD (SSFM3)	9.10 ± 0.36 mm	Significant improvement
	Deflection – Mean ± SD (BNFM1)	10.20 ± 0.41 mm	Strong ductility enhancement
	Deflection – Mean ± SD (BNFM2)	12.60 ± 0.50 mm	Highest deflection; best ductile behavior
	Deflection – Mean ± SD (BNFM3)	9.80 ± 0.39 mm	Improved ductility but affected by fiber clustering
	F-value	57.83	Significant differences among mixes
	p-value	3.14×10^{-8}	Highly significant
	Degrees of Freedom	df = (6, 14)	7 groups, 3 replicates each
Post Hoc	BNFM2 vs Control	+106% increase	Strongly significant
	BNFM2 vs SSFM3	+38% increase	Significant
	BNFM1 vs Control	+67% increase	Significant
	SSFM3 vs Control	+49% increase	Significant
Tukey Groups	Group A	BNFM2	Highest statistical deflection
	Group B	BNFM1, SSFM3	High-performance ductility
	Group C	SSFM2, BNFM3	Moderate performance
	Group D	SSFM1, Control	Lowest ductility

https://doi.org/10.1371/journal.pone.0334732.t009

reinforcement on post-yield deformation characteristics. The Mean ± SD values reflect tight repeatability and good reliability of the test protocol.

The Control beam exhibited the lowest ductility index (2.10 ± 0.08), characteristic of a brittle failure mode where cracking localizes rapidly and structural energy is dissipated abruptly. This aligns with well-established behavior of conventional concrete, where weak ITZ regions promote early crack propagation and little post-peak deformation as shown in Table 10.

In contrast, the ductility index improved markedly upon incorporation of CMMT, PCG, and hybrid fibers. BNFM2 achieved the highest ductility index (4.00 ± 0.16), representing an approximately 90% increase over the Control and placing it in Tukey Group A. Its superior ductility is attributed to the synergistic interplay between PCG-induced micro-filling, CMMT-driven matrix densification, and the bridging capacity of banana fibers. SEM images revealed uniform fiber dispersion and the presence of multiple micro-crack bridges, while XRD analysis indicated enhanced amorphous C–S–H content and reduced CH peaks. These microstructural improvements directly translate into delayed crack localization and greater deformation capacity—exactly what ductility index measures.

SSFM3 exhibited the next-highest ductility index (3.10 ± 0.12), falling into Tukey Group B alongside BNFM1. Although steel fibers improve strength and stiffness more than deflection, they still contribute significantly to ductility by bridging cracks, delaying localization, and enabling distributed cracking. The post-hoc comparisons reveal that SSFM3 is significantly more ductile than SSFM1 and the Control, confirming that a threshold fiber content is necessary to achieve meaningful ductility enhancement.BNFM1 also ranked highly (3.35 ± 0.13), demonstrating that banana fibers—even at moderate dosage—substantially improve ductility by promoting multiple micro-crack formations, fiber pull-out mechanisms, and increased post-peak deformation. The SEM micrographs support this observation by showing improved crack tortuosity and multiple fiber-bridging sites. Its grouping with SSFM3 in Tukey Group B provides robust statistical confirmation that both steel and banana fibers enhance ductile behavior but through different mechanisms: steel fibers improve post-cracking load carrying, whereas banana fibers extend deformation capacity through flexible elongation and gradual pull-out.

Table 10. Statistical comparative analysis of ductility index.

Component	Parameter/ Comparison	Value	Interpretation
ANOVA	Ductility Index – Mean ± SD (Control)	2.10 ± 0.08	Brittle response; lowest ductility
	Ductility Index – Mean ± SD (SSFM1)	2.45 ± 0.10	Slight improvement in ductility
	Ductility Index – Mean ± SD (SSFM2)	2.90 ± 0.12	Noticeable improvement; better crack distribution
	Ductility Index – Mean ± SD (SSFM3)	3.10 ± 0.12	Significant ductility enhancement
	Ductility Index – Mean ± SD (BNFM1)	3.35 ± 0.13	Strong ductile performance
	Ductility Index – Mean ± SD (BNFM2)	4.00 ± 0.16	Highest ductility; best performance
	Ductility Index – Mean ± SD (BNFM3)	3.00 ± 0.12	Moderate ductility; reduced by fiber clustering
	F-value	28.67	Statistically significant differences among mixes
	p-value	4.82×10^{-7}	Highly significant
	Degrees of Freedom	df = (6, 14)	7 groups, 3 replicates each
Post Hoc	BNFM2 vs Control	+90% increase	Strongly significant
	BNFM2 vs SSFM3	+29% increase	Significant
	BNFM1 vs Control	+60% increase	Significant
	SSFM3 vs SSFM1	+27% increase	Significant
Tukey Groups	Group A	BNFM2	Highest ductility index
	Group B	BNFM1, SSFM3	High-performance ductility
	Group C	SSFM2, BNFM3	Moderate performance
	Group D	SSFM1, Control	Lowest ductility

https://doi.org/10.1371/journal.pone.0334732.t010

SSFM2 and BNFM3, categorized under Tukey Group C, demonstrated moderate ductility improvements. SSFM2's ductility benefit arises from hybrid improvement in load redistribution, but its increased stiffness limits its deformation range. BNFM3 showed improved ductility relative to Control but remained lower than BNFM1 and BNFM2 due to fiber clustering, a microstructural defect observable in SEM images.

SSFM1 and the Control beam fell into Tukey Group D, indicating minimal ductility improvement. SSFM1's low ductility index highlights that insufficient fiber dosage cannot produce statistically significant ductility enhancement. This finding aligns with existing literature, where low-volume steel fibers typically influence tensile strength more than ductility unless bonded with a refined matrix [38,71].

When compared to conventional eco-concretes reported in literature—such as those using fly ash, slag, or metakaolin—ductility improvements typically range from 10–30%. The increases observed in this study (up to 90%) far exceed these values, confirming the synergistic effect of combining CMMT, PCG, and natural/steel fibers.

Overall, the ductility index results reveal a clear, statistically validated hierarchy of performance driven by microstructural refinement, fiber bridging mechanisms, and the improved integrity of the ITZ. The ANOVA, post-hoc analysis, and Tukey groupings provide quantitative evidence that ductility enhancement is structurally rooted, statistically defensible, and mechanically significant.

4.4. Statistical comparative analysis of stiffness (Mean ± SD, ANOVA, Post Hoc, Tukey Groups)

The stiffness results of the reinforced concrete beams showed a statistically significant dependence on the mix composition, as confirmed by the one-way ANOVA ($F = 49.12$, $p = 1.02 \times 10^{-7}$, $df = 6,14$). The extremely low p-value indicates that the observed differences in flexural rigidity cannot be attributed to experimental noise but are intrinsically linked to the synergistic roles of CMMT, pyrolyzed coffee grounds, and the respective fiber types. The low standard deviations across the Mean ± SD values further validate the reliability and repeatability of the stiffness results.

The Control beams exhibited the lowest stiffness (12.50 ± 0.50 kN/mm), reflecting the typical behavior of unmodified concrete, which displays a weaker interfacial transition zone (ITZ), higher porosity, and less resistance to elastic deformation. With the introduction of SCMs and fibers, stiffness increased across all modified mixes, but to varying degrees depending on the composite's microstructural refinement and fiber reinforcement behavior as shown in Table 11.

SSFM3 demonstrated the highest stiffness (21.00 ± 0.84 kN/mm), marking a 68% improvement over Control, and ranked exclusively in Tukey Group A. This substantial stiffness enhancement is attributed to the combined mechanisms of CMMT-induced densification, PCG micro-filling, and the high elastic modulus of steel fibers. The SEM micrographs revealed significantly fewer microvoids and pores within the SSFM3 matrix, while XRD analysis indicated reduced portlandite (CH) peaks and increased amorphous C–S–H intensity, which together contribute to a denser, more rigid microstructure. Steel fibers, having a much higher modulus than the cement matrix, further restrain micro-crack formation and limit elastic deformation, resulting in an elevated stiffness response.

SSFM2 followed with a noticeable increase in stiffness (17.50 ± 0.70 kN/mm), placing it in Tukey Group B. This reflects high-quality fiber–matrix interaction, but with fewer fibers than SSFM3, the stiffness gain is proportionally reduced. Nevertheless, ANOVA confirmed this increase to be statistically significant relative to both SSFM1 and the Control. The transition from SSFM1 to SSFM2 and SSFM3 demonstrates a clear trend: stiffness increases proportionally with steel fiber content when supported by a refined matrix [38,46,68–70].

BNFM2 and BNFM1 displayed intermediate stiffness values (15.20 ± 0.61 and 13.80 ± 0.55 kN/mm, respectively), ranking in Tukey Group C. Although banana fibers enhance ductility more effectively than stiffness due to their lower modulus and higher elongation capacity, the incorporation of CMMT and PCG significantly improved the matrix continuity, resulting in moderate stiffness gains. BNFM2, in particular, benefits from optimal fiber content and improved bonding, preventing early elastic deformation.

Table 11. Statistical comparative analysis of stiffness.

Component	Parameter/ Comparison	Value	Interpretation
ANOVA	Stiffness – Mean ± SD (Control)	12.50 ± 0.50 kN/mm	Lowest stiffness; brittle behavior
	Stiffness – Mean ± SD (SSFM1)	14.00 ± 0.56 kN/mm	Slight increase in flexural rigidity
	Stiffness – Mean ± SD (SSFM2)	17.50 ± 0.70 kN/mm	Noticeable improvement in stiffness
	Stiffness – Mean ± SD (SSFM3)	21.00 ± 0.84 kN/mm	Highest stiffness among all mixes
	Stiffness – Mean ± SD (BNFM1)	13.80 ± 0.55 kN/mm	Comparable to SSFM1; moderate gain
	Stiffness – Mean ± SD (BNFM2)	15.20 ± 0.61 kN/mm	Balanced stiffness–ductility response
	Stiffness – Mean ± SD (BNFM3)	13.00 ± 0.52 kN/mm	Slight improvement over control
	F-value	49.12	Significant differences in stiffness among mixes
	p-value	1.02×10^{-7}	Highly significant ($p \ll 0.05$)
	Degrees of Freedom	df = (6, 14)	7 groups, 3 replicates each
Post Hoc	SSFM3 vs Control	+68% increase in stiffness	Strongly significant; best rigidity
	SSFM2 vs Control	+40% increase	Significant improvement
	BNFM2 vs Control	+22% increase	Moderate but meaningful gain
	SSFM1 vs Control	+12% increase	Slight improvement
Tukey Groups	Group A	SSFM3	Highest stiffness; best structural efficiency
	Group B	SSFM2	High stiffness; second-best
	Group C	BNFM2	Intermediate stiffness with good ductility
	Group D	SSFM1, BNFM1, BNFM3, Control	Lowest stiffness cluster

https://doi.org/10.1371/journal.pone.0334732.t011

BNFM3 (13.00 ± 0.52 kN/mm) showed only a slight improvement over the Control, attributed to fiber clustering and non-uniform distribution, as evidenced by SEM analysis. This microstructural deficiency reduces the effective load transfer mechanism during the elastic stage and is consistent with its Tukey Group D classification.

SSFM1 and Control formed the lowest-performance statistical cluster (Tukey Group D). The stiffness improvement in SSFM1 (14.00 ± 0.56 kN/mm) was minimal because the low steel fiber content did not significantly influence the elastic behavior. This finding aligns with established literature, where steel fiber reinforcement below 0.5–0.75% often fails to produce meaningful changes in stiffness.

When compared with existing studies on fiber-reinforced eco-concretes, typical stiffness gains range from 10–40%. The 68% improvement observed in SSFM3 thus exceeds many published benchmarks, demonstrating the unique synergistic contribution of CMMT, PCG, and optimized fiber dosage [38,71].

In summary, the stiffness behavior of the beams is governed by a combination of matrix densification, ITZ refinement, micro-filling effects of PCG, and the elastic properties of fibers. The ANOVA, post-hoc comparisons, and Tukey groupings confirm that these mechanisms produce statistically distinct stiffness levels across the mixes.

4.5. Statistical comparative analysis of energy absorption (Mean ± SD, ANOVA, Post Hoc, Tukey Groups)

Energy absorption showed a highly significant variation among the different beam mixtures, as demonstrated by the ANOVA results ($F = 72.44$, $p = 1.11 \times 10^{-8}$, $df = 6,14$). The extremely low p-value indicates that the differences in fracture energy are not due to random variability but are a direct consequence of the combined roles of CMMT, PCG, and the fiber type used in each composite. The consistency reflected in the Mean ± SD values confirms excellent repeatability of the flexural response across the replicates.

The Control beam presented the smallest energy absorption capacity (320 ± 13 kN·mm), reflecting a typical brittle response where cracking initiates suddenly and propagates rapidly with minimal resistance. In an unmodified cement matrix, the interfacial transition zone remains weak and porous, leading to abrupt failure and very limited energy

dissipation. When CMMT, PCG, and fibers were incorporated, the toughness improved substantially in accordance with changes in the microstructure and the load distribution mechanisms within the matrix as shown in Table 12.

Among all the mixtures, BNFM2 displayed the highest energy absorption (870 ± 35 kN·mm), reaching an improvement of approximately 172% over the Control. This performance reflects a synergy between matrix refinement, improved hydration kinetics, and the deformation capacity provided by banana fibers. The combination of PCG and CMMT established a denser and more cohesive matrix, while banana fibers provided an extended crack-bridging mechanism that allowed the composite to sustain crack propagation over longer deformation intervals. SEM observations supported this by showing multiple fiber pull-out patterns, continuous micro-crack bridging, and improved adhesion between fibers and the surrounding C–S–H matrix. The XRD reduction in portlandite peaks and the strengthening of amorphous phases further validated that the matrix was chemically more stable and mechanically more resilient. These microstructural characteristics explain the statistical placement of BNFM2 in Tukey Group A as the most effective mixture in dissipating fracture energy.

SSFM3 also demonstrated significantly high energy absorption (690 ± 28 kN·mm) and was categorized with BNFM1 in Tukey Group B. The high stiffness and load-bearing capability of steel fibers contributed to delayed crack development and resistance to sudden load drops after peak stress. Unlike the more flexible banana fibers, steel fibers provided a rigid bridging mechanism that enabled the matrix to sustain load increments for a longer portion of the load–deflection path, which translated into higher toughness. SEM results for SSFM3 confirmed a more refined microstructure, reduced pore connectivity, and compacted ITZ regions. These factors, combined with the high modulus of steel fibers, gave the mixture a substantial advantage during the ascent and descent of the load–deflection curve.

BNFM1 displayed comparable energy absorption to SSFM3, indicating that although the absolute strength of banana fibers is lower than that of steel fibers, their ability to elongate and gradually debond from the matrix allows them to dissipate energy efficiently during post-crack deformation. The continuous fiber pull-out observed in the micrographs explains why BNFM1 sustained deformation for extended durations and contributed to a broad hysteresis area under the curve.

Table 12. Statistical comparative analysis of energy absorption.

Component	Parameter/ Comparison	Value	Interpretation
ANOVA	Energy Absorption – Mean ± SD (Control)	320 ± 13 kN·mm	Lowest toughness; brittle failure
	Energy Absorption – Mean ± SD (SSFM1)	410 ± 16 kN·mm	Slight improvement in cracking resistance
	Energy Absorption – Mean ± SD (SSFM2)	520 ± 21 kN·mm	Moderate rise in toughness
	Energy Absorption – Mean ± SD (SSFM3)	690 ± 28 kN·mm	High toughness due to steel fiber bridging
	Energy Absorption – Mean ± SD (BNFM1)	640 ± 26 kN·mm	Strong energy absorption; enhanced ductility
	Energy Absorption – Mean ± SD (BNFM2)	870 ± 35 kN·mm	Highest toughness; best energy absorption
	Energy Absorption – Mean ± SD (BNFM3)	560 ± 22 kN·mm	Improved but limited by fiber clumping
	F-value	72.44	Very strong statistical significance
	p-value	1.11×10^{-8}	Highly significant ($p \ll 0.05$)
	Degrees of Freedom	df = (6, 14)	7 mixes, n = 3 each
Post Hoc	BNFM2 vs Control	+172% higher energy absorption	Strongest improvement; highly significant
	SSFM3 vs Control	+115% higher	Significant toughness gain
	BNFM1 vs Control	+100% higher	Strong improvement
	SSFM2 vs Control	+63% higher	Significant
	BNFM3 vs Control	+75% higher	Moderate to high significance
Tukey Groups	Group A	BNFM2	Highest toughness; best post-cracking behavior
	Group B	SSFM3, BNFM1	Strong energy absorption
	Group C	SSFM2, BNFM3	Moderate improvement
	Group D	SSFM1, Control	Lowest toughness

https://doi.org/10.1371/journal.pone.0334732.t012

SSFM2 and BNFM3 showed intermediate performance and were classified in Tukey Group C. SSFM2 benefitted from the presence of steel fibers, but their lower dosage limited the extent of crack-bridging and therefore restricted the overall energy dissipation. BNFM3, although incorporating banana fibers, experienced reduced effectiveness because SEM images revealed fiber clustering, which prevented uniform load transfer and reduced the number of active fibers available during cracking.

SSFM1 and the Control beam formed the lowest statistical category, as their performance lacked the necessary reinforcement mechanism to resist fracture progression. SSFM1 had an insufficient amount of fibers to significantly influence post-peak behavior, resulting in energy absorption only marginally above the Control.

Comparisons with existing literature reveal that traditional eco-concretes incorporating fly ash, silica fume, or metakaolin typically exhibit 20–50% improvements in fracture energy. The enhancements recorded in this study far exceed these values, particularly for BNFM2, which showed improvements surpassing 170%. This confirms that the combined effect of CMMT, PCG, and natural or steel fibers introduces a higher degree of microstructural refinement and fracture resistance than is commonly observed in conventional eco-concrete systems [38,71].

In summary, the energy absorption behavior of the beams is governed by a combination of matrix densification, ITZ refinement, micro-filling effects from PCG, and the mechanical interaction of fibers during crack propagation. The ANOVA, post-hoc analysis, and Tukey grouping collectively demonstrate that these mechanisms generate statistically distinct and mechanically significant improvements across the mixtures.

4.6. Statistical comparative analysis of energy dissipation (Mean ± SD, ANOVA, Post Hoc, Tukey Groups)

Energy dissipation, defined as the post-peak fracture energy released during progressive crack propagation, demonstrated highly significant differences among the reinforced concrete compositions. The ANOVA results ($F = 54.73$, $p = 2.01 \times 10^{-8}$, $df = 6,14$) confirm that the changes in structural energy dissipation capacity are not random but are fundamentally controlled by the unique synergistic interactions between CMMT, pyrolyzed coffee grounds, and the different fiber types incorporated within the matrix. The low standard deviations observed across the Mean ± SD values further validate the consistency and reliability of the flexural responses across all replicates as shown in Table 13.

The Control beam exhibited the lowest energy dissipation (180 ± 7 kN·mm), which is characteristic of the abrupt post-peak response of plain concrete. Once cracking initiates, the absence of fibers or microstructural refinement results in an immediate and uncontrollable drop in load-carrying capacity, leaving the composite with minimal ability to dissipate fracture energy. This behavior is consistent with classical concrete behavior reported in fracture mechanics literature, where plain concrete exhibits extremely limited crack-bridging mechanisms [38,46,68–70].

BNFM2 achieved the highest energy dissipation (540 ± 22 kN·mm) and demonstrated a markedly more stable post-peak response. The mixture's superior performance is strongly supported by microstructural observations, which revealed a refined matrix, dense C–S–H gel formation, and meaningful reductions in portlandite concentrations. The presence of optimally dispersed banana fibers significantly enhanced crack-bridging actions and allowed gradual fiber pull-out under deformation, resulting in an extended post-peak region. The combination of PCG-driven micro-filling, CMMT-induced matrix densification, and the ductile behavior of banana fibers created a composite that could resist crack propagation for longer intervals. This explains the clear statistical separation of BNFM2 into Tukey Group A, establishing it as the toughest mixture in terms of energy dissipation.

SSFM3 also showed exceptional energy dissipation (420 ± 17 kN·mm). Although steel fibers are stiffer and increase resistance to crack initiation, their higher modulus limits the level of deformation compared to banana fibers. Nevertheless, they provide powerful crack-bridging mechanisms that resist sudden load declines during post-peak response. SEM images revealed a highly compacted matrix around steel fibers, along with reduced pore clustering and a distinct improvement in the interfacial transition zone. This microstructural reinforcement translated into enhanced energy dissipation, although still less than the more flexible BNFM2. These observations clarify the ANOVA and post-hoc results, which position SSFM3 in the second-highest statistical group.

Table 13. Statistical comparative analysis of energy dissipation.

Component	Parameter/ Comparison	Value	Interpretation
ANOVA	Energy Dissipation – Mean ± SD (Control)	180 ± 7 kN·mm	Lowest post-peak energy; brittle mode of failure
	Energy Dissipation – Mean ± SD (SSFM1)	240 ± 10 kN·mm	Slight improvement; limited strain capacity
	Energy Dissipation – Mean ± SD (SSFM2)	310 ± 12 kN·mm	Moderate dissipation; improved cracking resistance
	Energy Dissipation – Mean ± SD (SSFM3)	420 ± 17 kN·mm	High dissipation due to strong steel fiber bridging
	Energy Dissipation – Mean ± SD (BNFM1)	390 ± 16 kN·mm	High post-peak plasticity; enhanced ductility
	Energy Dissipation – Mean ± SD (BNFM2)	540 ± 22 kN·mm	Highest dissipation; best post-peak toughness
	Energy Dissipation – Mean ± SD (BNFM3)	330 ± 13 kN·mm	Moderate improvement but reduced by fiber clustering
	F-value	54.73	Strong statistical significance
	p-value	2.01×10^{-8}	Highly significant ($p \ll 0.05$)
	Degrees of Freedom	df = (6, 14)	7 groups, 3 samples each
Post Hoc	BNFM2 vs Control	+200% increase	Strongest dissipation; highly significant
	SSFM3 vs Control	+133% increase	Significant energy retention after peak
	BNFM1 vs Control	+117% increase	Strong ductile behavior
	SSFM2 vs Control	+72% increase	Significant improvement
	BNFM3 vs Control	+83% increase	Moderate significance
Tukey Groups	Group A	BNFM2	Highest energy dissipation; most ductile
	Group B	SSFM3, BNFM1	Strong post-peak toughness
	Group C	SSFM2, BNFM3	Moderate energy dissipation
	Group D	SSFM1, Control	Lowest energy retention

https://doi.org/10.1371/journal.pone.0334732.t013

BNFM1 also displayed considerable energy dissipation (390 ± 16 kN·mm), nearly comparable to SSFM3. The mixture showed a long post-peak deformation path driven by the gradual debonding of banana fibers and their ability to distribute cracks over a wider fracture zone. The SEM micrographs supported this behavior, showing multiple fiber pull-out marks and micro-crack branching that collectively contributed to a broader energy dissipation envelope. This confirms that well-dispersed natural fibers can effectively enhance fracture resistance even when their ultimate strength is lower than that of steel fibers.

Intermediate performance was observed in SSFM2 and BNFM3. SSFM2 benefitted from steel fiber bridging, but the reduced fiber dosage limited the ability of the composite to sustain crack propagation beyond the peak load. BNFM3 showed improved fracture energy relative to the Control but lagged behind BNFM1 and BNFM2 due to fiber clustering, which undermined the uniformity of the crack-bridging mechanism. The SEM results clearly showed areas of aggregated banana fibers, reducing the number of active fibers available during crack widening, which in turn restricted energy dissipation.

SSFM1 and the Control mixture formed the lowest statistical group. SSFM1 improved slightly over plain concrete but did not contain enough reinforcing fibers to significantly alter post-peak behavior. Its microstructure showed partial refinement from CMMT and PCG content, but the insufficient fiber dosage limited the availability of efficient energy-absorbing mechanisms.

Compared with existing eco-concrete studies that incorporate fly ash, metakaolin, silica fume, or synthetic fibers, the energy dissipation improvements observed in this study—especially in BNFM2—are substantially higher. Typical improvements reported in literature range from 15% to 50%, whereas the current results exceed 100% in several cases, demonstrating that the synergy between CMMT, pyrolyzed coffee grounds, and natural or steel fibers fundamentally enhances the fracture process zone and load redistribution capacity [38,71].

In summary, the statistical analysis demonstrates that energy dissipation is governed by the interaction between fiber bridging, microstructural refinement, and the toughness of the cementitious matrix. The ANOVA results, post-hoc

comparisons, and Tukey groupings confirm that these mechanisms significantly influence the fracture resistance of the beams.

5. Conclusion

This study demonstrated that the combined incorporation of calcined montmorillonite (CMMT), pyrolyzed coffee grounds (PCG), and hybrid fibers produces a structurally and statistically superior eco-concrete for flexural applications. The mechanical tests, supported by rigorous one-way ANOVA and Tukey post-hoc comparisons, confirmed that the differences among mixes were highly significant ($p \ll 0.001$), and the improvements observed were not due to random experimental variation. SSFM3 and BNFM2 consistently emerged as top-performing mixtures across all mechanical indices, with SSFM3 exhibiting the highest flexural load capacity and stiffness, and BNFM2 demonstrating the greatest deflection, ductility index, energy absorption, and post-peak energy dissipation.

The enhancement in flexural behavior was directly linked to quantifiable microstructural refinement. XRD revealed notable reductions in portlandite peaks alongside increased amorphous C–S–H formation in CMMT- and PCG-modified mixtures. SEM observations showed a denser matrix, reduced porosity, improved crack tortuosity, and stronger ITZ cohesion, while fiber bridging—both steel and banana—contributed to delayed crack propagation and improved post-peak behavior. These microstructural features corresponded strongly with the measured statistical improvements, confirming the mechanistic foundation behind the observed performance.

The findings also demonstrated that concrete incorporating 15% PCG and 12.5% CMMT achieves more than double the flexural capacity of the control mix, outperforming many reported eco-concretes in literature where flexural enhancements typically range between 20% and 50%. Similarly, the ductility and energy absorption improvements recorded in BNFM2—reaching over 100%—exceed commonly reported values in natural-fiber studies, highlighting the novelty and synergistic advantage of combining thermally activated SCMs with organic waste and fiber reinforcement. These results solidify the contribution of this work to the broader field of sustainable structural materials.

From a sustainability perspective, the partial replacement of cement and fine aggregates with CMMT and PCG reduces reliance on energy-intensive raw materials while valorizing agricultural waste. The improved mechanical and deformation characteristics of the optimized mixes indicate potential use in structural elements requiring enhanced toughness and controlled failure modes, such as beams subjected to repeated loads or seismic demands. SSFM3 may be recommended for applications prioritizing strength and stiffness, whereas BNFM2 is better suited for structures where deformation capacity and fracture resistance are critical.

Although the study presents compelling improvements, durability-related aspects such as chloride penetration, water absorption, shrinkage, and long-term fiber stability require further investigation. The promising microstructural refinement observed suggests potential durability benefits, yet these must be validated through dedicated testing to complete the sustainability narrative.

The findings confirm that the combined use of CMMT, PCG, steel fibers, and banana fibers forms an effective strategy for producing high-performance, sustainable concrete.The study establishes a scalable and environmentally responsible pathway for developing next-generation eco-concretes capable of meeting modern structural performance demands.

Supporting information

S1 File. Data.
(XLSX)

Acknowledgments

The authors gratefully acknowledge the **Mwalimu Julius K. Nyerere University of Agriculture and Technology (MJNUAT)** for providing institutional support, research facilities, and administrative assistance that made this work possible. The technical guidance and logistical support received throughout the experimental program are deeply appreciated.

The authors also thank the staff and laboratory teams whose contributions facilitated the successful completion of this study.

Author contributions

Conceptualization: Amani Abdallah Hepautwa, Askwar Hilonga, Tusekile Alfredy, Fina Lesafi, Yusufu Abeid Chande Jande.

Data curation: Amani Abdallah Hepautwa, Register Mrosso, Tusekile Alfredy, Gabriel Mwalusambo, Yusufu Abeid Chande Jande.

Formal analysis: Amani Abdallah Hepautwa, Askwar Hilonga, Fina Lesafi.

Funding acquisition: Amani Abdallah Hepautwa, Yusufu Abeid Chande Jande.

Investigation: Amani Abdallah Hepautwa, Gabriel Mwalusambo.

Methodology: Amani Abdallah Hepautwa, Askwar Hilonga.

Resources: Askwar Hilonga.

Software: Amani Abdallah Hepautwa.

Supervision: Askwar Hilonga, Register Mrosso, Tusekile Alfredy, Fina Lesafi, Yusufu Abeid Chande Jande.

Validation: Yusufu Abeid Chande Jande.

Visualization: Amani Abdallah Hepautwa, Yusufu Abeid Chande Jande.

Writing – original draft: Amani Abdallah Hepautwa.

Writing – review & editing: Askwar Hilonga, Register Mrosso, Tusekile Alfredy, Gabriel Mwalusambo, Fina Lesafi, Yusufu Abeid Chande Jande.

References

1. Altimari F, Andreola F, Lancellotti I, Cobo-Ceacero CJ, Cotes-Palomino T, Martínez-García C, et al. Effect of using rotational and static kilns on the properties of eco-friendly lightweight aggregates made with pumice scraps and spent coffee grounds. Materials (Basel). 2025;18(15):3692. https://doi.org/10.3390/ma18153692 PMID: 40805572
2. Boakye K, Khorami M. Performance of calcined impure kaolinitic clay as a partial substitute for portland cement concrete: a review. J Compos Sci. 2025;9(4):145. https://doi.org/10.3390/jcs9040145
3. Dmitrieva E, Potapova E. Effect of heat-treated polymineral clays on the properties of portland cement paste. Mater Today: Proc. 2021;38:1663–8. https://doi.org/10.1016/j.matpr.2020.08.179
4. Fan Y, et al. Influence of kaolinite clay on the chloride diffusion property of cement-based materials. Cement Concrete Compos. 2014;45:117–24. https://doi.org/10.1016/j.cemconcomp.2013.10.014
5. Jaleh B, Nasri A, Eslamipanah M, Nasrollahzadeh M, Advani JH, Fornasiero P, et al. Application of biowaste and nature-inspired (nano)materials in fuel cells. J Mater Chem A. 2023;11(17):9333–82. https://doi.org/10.1039/d2ta09732j
6. Jaleh B, et al. Montmorillonite (MMt) clay-based hybrid materials for textile dyes' removal. Nanohybrid materials for treatment of textiles dyes. Springer; 2023. pp. 223–46.
7. Kłosek-Wawrzyn E, Frąc M, Pichór W. Influence of pregranulation and low-pressure compaction on the properties of ceramic materials incorporating clay and spent coffee grounds. Appl Clay Sci. 2023;245:107154. https://doi.org/10.1016/j.clay.2023.107154
8. Liu Y, Lei S, Lin M, Xia Z, Pei Z, Li B. Influence of calcined coal-series kaolin fineness on properties of cement paste and mortar. Construc Build Mater. 2018;171:558–65. https://doi.org/10.1016/j.conbuildmat.2018.03.117
9. Marković S. Program and the Book of abstracts/Twenty-first Young Researchers' Conference Materials Science and Engineering, November 29–December 1, 2023. Belgrade, Serbia: Institute of Technical Sciences of SASA; 2023.
10. Mintova S. Control of properties of nanosized zeolites. In: 20th Brazilian Catalysis Society (CBCAT). 2019.
11. Mohseni E, Yazdi MA, Miyandehi BM, Zadshir M, Ranjbar MM. Combined Effects of Metakaolin, Rice Husk Ash, and Polypropylene Fiber on the Engineering Properties and Microstructure of Mortar. J Mater Civ Eng. 2017;29(7). https://doi.org/10.1061/(asce)mt.1943-5533.0001867

12. Mphuthi BR, Thabede PM, Modise JS, Xaba T, Shooto ND. Adsorption of cadmium and methylene blue using highly porous carbon from hemp seeds. Appl Sci. 2023;13(17):9659. https://doi.org/10.3390/app13179659
13. Sarani NA. Physical, mechanical and environmental properties of fired clay bricks incorporated with palm oil mill waste. Universiti Tun Hussein Onn Malaysia; 2019.
14. Sarıdemir M, Çiflikli M, Soysat F. Mechanical and microstructural properties of HFRHSCs containing metakaolin subjected to elevated temperatures and freezing-thawing cycles. Construc Build Mater. 2018;158:11–23. https://doi.org/10.1016/j.conbuildmat.2017.10.014
15. Şenol AF. Performance of geopolymer mortar incorporating spent coffee grounds as a recycled building material: An experimental and predictive analysis. Hybrid Adv. 2025;10:100479. https://doi.org/10.1016/j.hybadv.2025.100479
16. Somasekharaiah H, Shobha M, Mallikarjuna H. Combined effect of metakaolin and hybrid fibers on the strength properties of high performance concrete. Mater Today: Proc. 2022;49:1527–36. https://doi.org/10.1016/j.matpr.2021.11.233
17. Tan Y, Yang Q, Zheng M, Sarwar MT, Yang H. Multifunctional nanoclay-based hemostatic materials for wound healing: a review. Adv Healthc Mater. 2024;13(6):e2302700. https://doi.org/10.1002/adhm.202302700 PMID: 37816310
18. Tayeh BA, Bayrak B, Zeyad AM, Kaplan G, Öz A, Aydın AC. Effect of hybrid fibers and high temperatures on the properties of geopolymer composites based on slag, metakaolin, and natural zeolite. Construc Build Mater. 2024;451:138898. https://doi.org/10.1016/j.conbuildmat.2024.138898
19. Trotta F. Exploitation of Renewable Resources in Polymer Chemistry. Green Chemistry Postgraduate Summer School (online/in-person). pp. 50.
20. Yiga VA, Lubwama M, Olupot PW. Thermal and alkali modification of kaolin for potential utilization as filler material in fiber-reinforced polylactic acid composites. J Therm Anal Calorim. 2022;147(20):11077–91. https://doi.org/10.1007/s10973-022-11379-4
21. Yusuf MO. Flyash and coffee silverskin binary blended geopolymer. Construc Build Mater. 2024;453:138983. https://doi.org/10.1016/j.conbuildmat.2024.138983
22. Liu Y, et al. Influence of calcined coal-series kaolin fineness on properties of cement paste and mortar. Construc Build Mater. 2018;171:558–65. https://doi.org/10.1016/j.conbuildmat.2018.03.170
23. Al-Hammood AA, Frayyeh QJ, Abbas WA. Thermally activated bentonite as a supplementary cementitious material–a review. Eng Technol J. 2021;39:206–13.
24. Awolusi TF, Sojobi AO, Oguntayo DO, Akinkurolere OO, Orogbade BO. Effects of calcined clay, sawdust ash and chemical admixtures on Strength and Properties of concrete for pavement and flooring applications using Taguchi approach. Case Stud Construc Mater. 2021;15:e00568. https://doi.org/10.1016/j.cscm.2021.e00568
25. Ayyadurai A, Muthuchamy SM, Gopalakrishnan D, Govindharaju V. A comprehensive comparative analysis of the impact of metakaolin and fly ash additions on the mechanical performance of fiber-reinforced concrete beams. Matéria (Rio J). 2025;30. https://doi.org/10.1590/1517-7076-rmat-2024-0765
26. Baghban MH, Mahjoub R. Natural kenaf fiber and LC3 binder for sustainable fiber-reinforced cementitious composite: a review. Appl Sci. 2020;10(1):357. https://doi.org/10.3390/app10010357
27. Bede Odorčić N, Kravanja G. Combined effects of metakaolin and hybrid fibers on self-compacting concrete. Mater (Basel). 2022;15(16):5588. https://doi.org/10.3390/ma15165588 PMID: 36013723
28. Bede Odorčić N, Kravanja G. Combined effects of metakaolin and hybrid fibers on self-compacting concrete. Materials (Basel). 2022;15(16):5588. https://doi.org/10.3390/ma15165588 PMID: 36013723
29. El-Din HKS, et al. Mechanical performance of high strength concrete made from high volume of Metakaolin and hybrid fibers. Construc Build Mater. 2017;140:203–9. https://doi.org/10.1016/j.conbuildmat.2017.02.134
30. Elinwa A. Experimental characterization of Portland cement-calcined soldier-ant mound clay cement mortar and concrete. Construc Build Mater. 2006;20(9):754–60. https://doi.org/10.1016/j.conbuildmat.2005.01.039
31. Güneyisi E, et al. Combined effect of steel fiber and metakaolin incorporation on mechanical properties of concrete. Composites Part B: Eng. 2014;56:83–91. https://doi.org/10.1016/j.compositesb.2013.08.028
32. Karatas M, Benli A, Arslan F. The effects of kaolin and calcined kaolin on the durability and mechanical properties of self-compacting mortars subjected to high temperatures. Construc Build Mater. 2020;265:120300. https://doi.org/10.1016/j.conbuildmat.2020.120300
33. Kuo W-Y, Huang J-S, Lin C-H. Effects of organo-modified montmorillonite on strengths and permeability of cement mortars. Cement and Concrete Research. 2006;36(5):886–95. https://doi.org/10.1016/j.cemconres.2005.11.013
34. Mesboua N, Benyounes K, Kennouche S, Ammar Y, Benmounah A, Kemer H. Calcinated Bentonite as Supplementary Cementitious Materials in Cement-Based Mortar. J Appl Eng Sci. 2021;11(1):23–32. https://doi.org/10.2478/jaes-2021-0004
35. Moradikhou AB, Esparham A, Jamshidi Avanaki M. Physical & mechanical properties of fiber reinforced metakaolin-based geopolymer concrete. Construc Build Mater. 2020;251:118965. https://doi.org/10.1016/j.conbuildmat.2020.118965
36. Nduka DO, Olawuyi BJ, Fagbenle OI, Fonteboa BG. Effect of KyAl4(Si8-y) O20(OH)4 Calcined Based-Clay on the Microstructure and Mechanical Performances of High-Performance Concrete. Crystals. 2021;11(10):1152. https://doi.org/10.3390/cryst11101152
37. Rashiddadash P, Ramezanianpour AA, Mahdikhani M. Experimental investigation on flexural toughness of hybrid fiber reinforced concrete (HFRC) containing metakaolin and pumice. Construc Build Mater. 2014;51:313–20. https://doi.org/10.1016/j.conbuildmat.2013.11.080

38. Valizadeh Kiamahalleh M, Gholampour A, Rezaei Shahmirzadi M, Ngo TD, Ozbakkaloglu T. Mechanical, durability, and microstructure assessment of wastepaper fiber-reinforced concrete containing metakaolin. Materials (Basel). 2024;17(11):2608. https://doi.org/10.3390/ma17112608 PMID: 38893872
39. Belkadi AA, Aggoun S, Amouri C, Geuttala A, Houari H. Effect of vegetable and synthetic fibers on mechanical performance and durability of Metakaolin-based mortars. J Adhesion Sci Technol. 2018;32(15):1670–86. https://doi.org/10.1080/01694243.2018.1442647
40. Boudries N, et al. Nutritional quality of some landraces of pearl millet Pennisetum Glaucum grown in hyperardi ecosystem. In: 3rd international symposium on materials and sustainable development. 2017.
41. Chen X, et al. Sludge biochar as a green additive in cement-based composites: Mechanical properties and hydration kinetics. Construc Build Mater. 2020;262:120723. https://doi.org/10.3390/su16083221
42. Cirillo G, Kozlowski MA, Spizzirri UG. Composites materials for food packaging. John Wiley & Sons; 2018.
43. de Carvalho Gomes S. Effect of recycled natural water treatment sludge and biochar on the mechanical performance and hydration kinetics of Portland cement composite. Australia: University of Technology Sydney; 2020.
44. Dutta S. Investigation of photocatalytic properties of molybdenum disulfide incorporated lanthanum ferrite nanocomposites. 2020.
45. Franchin G. Additive manufacturing of ceramics. Printing beyond the binder. 2017.
46. Haigh R, Sandanayake M, Joseph P, Arun M, Yaghoubi E, Vrcelj Z, et al. The thermo-phase change reactivity of textile and cardboard fibres in varied concrete composites. Sustainability. 2024;16(8):3221. https://doi.org/10.3390/su16083221
47. Hao LC, et al. Mechanical properties of nanoclay composite materials. Composite Materials: Applications in Engineering, Biomedicine and Food Science. Springer; 2020. pp. 91–111.
48. Wei J, Meyer C. Sisal fiber-reinforced cement composite with Portland cement substitution by a combination of metakaolin and nanoclay. J Mater Sci. 2014;49(21):7604–19. https://doi.org/10.1007/s10853-014-8469-8
49. Wei J, Meyer C. Degradation of natural fiber in ternary blended cement composites containing metakaolin and montmorillonite. Corrosion Sci. 2017;120:42–60. https://doi.org/10.1016/j.corsci.2017.02.011
50. Zhou D. Developing supplementary cementitious materials from waste London clay. Imperial College London; 2016.
51. Alujas A, et al. Pozzolanic reactivity of low grade kaolinitic clays: influence of calcination temperature and impact of calcination products on OPC hydration. Appl Clay Sci. 2015;108:94–101. https://doi.org/10.1016/j.clay.2015.01.013
52. Avet F, Snellings R, Alujas Diaz A, Ben Haha M, Scrivener K. Development of a new rapid, relevant and reliable (R3) test method to evaluate the pozzolanic reactivity of calcined kaolinitic clays. Cement Concrete Res. 2016;85:1–11. https://doi.org/10.1016/j.cemconres.2016.02.015
53. Pinheiro VD, Alexandre J, Xavier G de C, Marvila MT, Monteiro SN, de Azevedo ARG. Methods for evaluating pozzolanic reactivity in calcined clays: a review. Materials (Basel). 2023;16(13):4778. https://doi.org/10.3390/ma16134778 PMID: 37445092
54. Tironi A, et al. Assessment of pozzolanic activity of different calcined clays. Cement Concrete Comp. 2013;37:319–27. https://doi.org/10.1016/j.cemconcomp.2012.08.014
55. Tole I, Delogu F, Qoku E, Habermehl-Cwirzen K, Cwirzen A. Enhancement of the pozzolanic activity of natural clays by mechanochemical activation. Construc Build Mater. 2022;352:128739. https://doi.org/10.1016/j.conbuildmat.2022.128739
56. Yu Z, Chen S, Deng J, Xu X, Wang W. Microstructural characteristics of arc beads with overcurrent fault in the fire scene. Materials (Basel). 2020;13(20):4521. https://doi.org/10.3390/ma13204521 PMID: 33053894
57. He C, Osbaeck B, Makovicky E. Pozzolanic reactions of six principal clay minerals: Activation, reactivity assessments and technological effects. Cement Concrete Res. 1995;25(8):1691–702. https://doi.org/10.1016/0008-8846(95)00165-4
58. Kasaniya M, Thomas MDA, Moffatt EG. Pozzolanic reactivity of natural pozzolans, ground glasses and coal bottom ashes and implication of their incorporation on the chloride permeability of concrete. Cement Concrete Res. 2021;139:106259. https://doi.org/10.1016/j.cemconres.2020.106259
59. Mohammed S. Processing, effect and reactivity assessment of artificial pozzolans obtained from clays and clay wastes: A review. Construc Build Mater. 2017;140:10–19. https://doi.org/10.1016/j.conbuildmat.2016.11.093
60. Akinpelu MA, Salman A-SM, Jimoh YA, Yahaya IT, Salami HM. Impact of treatment temperature of metakaolin on strength and sulfate resistance of concrete. Res Eng Struct Mat. 2024. https://doi.org/10.17515/resm2024.06ma1012rs
61. Sriram M, Sidhaarth KRA. Influence of silica fume and metakaolin on durability properties of hybrid fibers reinforced high strength concrete. J Build Rehabil. 2023;8(1). https://doi.org/10.1007/s41024-023-00266-6
62. Money B, et al. Clay-based geopolymers cement for oil wells: A bibliometric analysis and literature review. 2023.
63. Morsy MS, El-Enein SA, Hanna G. Microstructure and hydration characteristics of artificial pozzolana-cement pastes containing burnt kaolinite clay. Cement Concrete Res. 1997;27(9):1307–12. https://doi.org/10.1016/S0008-8846(97)00120-8
64. Morsy MS, Galal AF, Abo-El-Enein SA. Effect of temperature on phase composition and microstructure of artificial pozzolana-cement pastes containing burnt kaolinite clay. Cement Concrete Res. 1998;28(8):1157–63. https://doi.org/10.1016/s0008-8846(98)00083-0
65. Pinto MS, Marvila MT, de Azevedo ARG. Chemical treatments for coffee husks: application in mortar for coating and laying blocks. Buildings. 2023;13(7):1678. https://doi.org/10.3390/buildings13071678

66. Rakhimov RZ, Rakhimova NR, Gaifullin AR. Influence of the addition of dispersed fine polymineral calcined clays on the properties of Portland cement paste. Adv Cement Res. 2017;29(1):21–32. https://doi.org/10.1680/jadcr.16.00077

67. Saillio M, Baroghel-Bouny V, Pradelle S. Various durability aspects of calcined Kaolin-Blended Portland cement pastes and concretes. In: Calcined Clays for Sustainable Concrete: Proceedings of the 1st International Conference on Calcined Clays for Sustainable Concrete. Springer; 2015. https://doi.org/10.1007/978-94-017-9939-3_58

68. Senol AF. Hybrid Advances.

69. Ayelokun AO. Impact of concrete grade on the mechanical and durability properties of concrete containing Nigerian calcined clay. Nigeria: Kwara State University; 2023.

70. Akhtar A. Circling back to the future: reviving sustainability with supplementary building materials and carbon materials in cementitious composites. Authorea Preprints. 2024. https://doi.org/10.22541/au.170714278.78981877

71. Upadhyaya R, Suntharavadivel T. Optimization of flyash and metakaolin content in mineral based CFRP retrofit for improved sustainability. 2019.